

Unified calibration and spatial mapping of fine particulate matter data from multiple low-cost air pollution sensor networks in Baltimore, Maryland

Claire Heffernan^{*1}, Kirsten Koehler^{†2}, Drew R. Gentner^{‡3}, Roger D. Peng^{§4},
Abhirup Datta^{*5}

Abstract

Low-cost air pollution sensor networks are increasingly being deployed globally, supplementing sparse regulatory monitoring with localized air quality data. In some areas, like Baltimore, Maryland, there are only few regulatory (reference) devices but multiple low-cost networks. While there are many available methods to calibrate data from each network individually, separate calibration of each network leads to conflicting air quality predictions. We develop a general Bayesian spatial filtering model combining data from multiple networks and reference devices, providing dynamic calibrations (informed by the latest reference data) and unified predictions (combining information from all

^{*}Department of Biostatistics, Johns Hopkins University, ¹cmheff@jhu.edu, ⁵abhidatta@jhu.edu

[†]Department of Environmental Health and Engineering, Johns Hopkins University, ²kkoehle1@jhu.edu

[‡]Department of Chemical & Environmental Engineering, Yale University, ³drew.gentner@yale.edu

[§]Department of Statistics and Data Sciences, University of Texas, Austin,

⁴roger.peng@austin.utexas.edu

available sensors) for the entire region. This method accounts for network-specific bias and noise (observation models), as different networks can use different types of sensors, and uses a Gaussian process (state-space model) to capture spatial correlations. We apply the method to calibrate $\text{PM}_{2.5}$ data from Baltimore in June and July 2023 – a period including days of hazardous concentrations due to wildfire smoke. Our method helps mitigate the effects of preferential sampling of one network in Baltimore, results in better predictions and narrower confidence intervals. Our approach can be used to calibrate low-cost air pollution sensor data in Baltimore and any other areas with multiple low-cost networks.

Keywords: Gaussian process, Bayesian statistics, Kalman filtering, low-cost networks, air pollution, spatial statistics

1 Introduction

Air pollution is a major concern worldwide. 6.5 million deaths per year worldwide are caused by air pollution (Fuller et al., 2022). The U.S. Environmental Protection Agency (EPA) has established guidelines for concentrations of major pollutants and has recently lowered the annual standard for fine particulate matter (PM_{2.5}) from 12 $\mu\text{g}/\text{m}^3$ to 9 $\mu\text{g}/\text{m}^3$ (U.S. EPA, 2024). The World Health Organization (WHO) estimates that 99% of people are exposed to higher concentrations of pollution than the guidelines (WHO, 2024).

In Baltimore, there is evidence that air pollution is not evenly distributed across the city (Boone et al., 2014). Therefore, it is important to understand the air quality throughout the entire city at a fine spatial scale. However, accurately measuring air quality is costly. The gold standard of air quality measurement are devices that meet the EPA’s standards, the Federal Reference Method (FRM) or Federal Equivalent Method (FEM). We call these devices *reference devices* because their measurements meet EPA’s requirements for accuracy and precision. States deploy networks of reference devices to record these high-quality measurements. However, these networks are often sparse; for example, Maryland only has 26 devices in the state, and only 1 in Baltimore (MDE, 2023). Thus, reference devices alone are not enough to give spatial information about air quality in Baltimore.

Low-cost sensors (LCS) are a solution to the sparsity of reference devices. These sensors usually cost a few hundred dollars, considerably less expensive than reference devices, and can be installed in many more locations within a city. Such networks exist in many areas, including many major cities in the United States (Kim et al., 2018; DeSouza et al., 2022; Esie et al., 2022). The PurpleAir network is one example of a low-cost air pollution network. It is a community science network where individuals can purchase a sensor to place outside

their homes to record air quality. PurpleAir data is publicly available for those who agree to share their data and there are sensors in many areas of the United States.

Low-cost sensors suffer from having bias and noise in the measurements, and must be calibrated before being used. One approach to calibration is field-calibration, where sensors are deployed and calibration equations are created based on the real-world performance of the sensors. To fit the calibration equations, some high-quality air pollution measurements are needed. Thus, some low-cost sensors can be placed in the same location as reference devices. These locations, with both a reference and low-cost sensor are called *collocated sites*, and the measurements at these sites can be used to create calibration equations. Using this collocated data, field-calibration is done by training and applying various types of regression models with the reference measurement as the outcome and the low-cost measurement and other meteorological variables as predictors (Barkjohn et al., 2021; Datta et al., 2020; Bigi et al., 2018; Bi et al., 2020; Ardon-Dryer et al., 2020; Si et al., 2020; Romero et al., 2020).

Recently, Heffernan et al. (2023) showed that regression-based field-calibration equations systematically underestimate high concentrations. Many of these approaches are also not spatially informed. To mitigate these issues, (Heffernan et al., 2023) proposed a spatial filtering model called the Gaussian Process Filter (GP Filter), reviewed in Section 3.1. The observation model part of GP Filter switches the roles of outcome and predictor variables from standard regression calibration, and models the low-cost measurements as a noisy and biased version of the true concentrations, as measured by the reference devices. The state-space model accounts for spatial structure in true pollutant levels and is specified as a conditional Gaussian process regression for the true concentrations given the reference data at a handful of locations. The GP Filter thus uses all the low-cost data available and the contemporary reference data to make dynamic spatially informed predictions. The approach was used to

calibrate $\text{PM}_{2.5}$ data from ~ 45 sensors of the SEARCH (Solutions to Energy, Air, Climate, and Health Center) low-cost network in Baltimore.

Besides the SEARCH network, the PurpleAir network also has considerable presence in Baltimore, with roughly 30 $\text{PM}_{2.5}$ sensors in the area. Utilizing this additional data can enrich our knowledge of intra-urban variations of $\text{PM}_{2.5}$ in Baltimore. However, we will illustrate that there is evidence of preferential sampling in the PurpleAir network, which would occur when sensors are more concentrated in areas with either higher or lower concentrations. Studies (Shaddick and Zidek, 2014; Lee et al., 2015) have shown that preferential sampling can lead to biased estimates of city-level or regional air quality. Thus, the PurpleAir network does not give an accurate assessment of air quality as a whole, and this data alone may not be the best approach for estimating air quality in Baltimore. Preferential sampling is less of a concern for the SEARCH network since sites are selected by using a weighted random sample to select a representative set of locations. However, the SEARCH network is more spread out, leaving large gaps in the city where predictions are imprecise.

Leveraging data from both the SEARCH and the PurpleAir networks in Baltimore has the potential to improve over either network individually. However, multiple low-cost networks in an area can have different biases and noise levels, since different brands of sensors from different manufacturers are made differently. For example, the PurpleAir network uses Plantower PMS5003 sensors, while the SEARCH network uses Plantower A003 sensors, two different types of devices from the same manufacturer whose inlets are designed differently. Therefore, the measurements made by the different networks are not directly comparable, and they should be treated as separate networks for the purpose of calibration, with the biases and noises of each each network addressed separately. However, most of the existing calibration methods for LCS networks do not address the setting of multiple low-cost networks

within an area. A simple approach would be to calibrate each network separately. However, naïve network-specific calibration followed by spatial interpolation would lead to different predicted air quality maps for the region using each network, with potentially conflicting predictions of air-quality from the networks thereby requiring some ad-hoc way to merge the two or more sets of predictions to create unified maps. It is more desirable to develop new methodology for coherent fusion of air pollution data coming from multiple networks.

We develop a principled statistical framework for network-specific calibration but unified prediction of air quality data from multiple LCS networks. We extend the spatial filtering approach of Heffernan et al. (2023) to joint modeling of data from multiple low-cost networks as well as the sparse reference network, sharing information across all the networks and locations. We deploy a hierarchical Bayesian model, the first-stages of which consist of separate observation models for each LCS network, modeling the LCS data as a biased and noisy version of the reference data with biases and noises being network-specific. A last-stage Gaussian Process based spatial state-space model specifies the spatial surface of the true concentrations which is informed by the available reference data at one or few locations. Like the single network GP filter, calibrations obtained from our method will be dynamic, i.e., informed by the latest reference data in the region. Additionally, our method offers three main advantages over calibrating each network individually: (1) it offers a principled approach to obtain unified set of spatial predictions of air quality at any location in the region that is informed by all available data (LCS networks as well as any available reference data), (2) it improves prediction accuracy, especially when some networks have preferential sampling, and (3) it generally reduces uncertainty around the predictions by using data from a denser set of locations by combining multiple networks. We present the method in Section 3.2. More details about the advantages are given in Section 3.3.

Section 4 applies the method to calibrate low-cost data from two LCS networks and one reference device in Baltimore. We train the model in Baltimore and investigate performance both at typical concentrations for Baltimore, and at unusually high concentrations due to smoke from wildfires. We also investigate the impact of preferential sampling in one of the networks. We validate our approach in simulations in Section 5.

2 Baltimore low-cost sensor air quality data networks

In Baltimore, Maryland, the PurpleAir network (Barkjohn et al., 2021) and the Solutions to Energy, Air, Climate, and Health (SEARCH) Center (Levy Zamora et al., 2018; Hefferman et al., 2023) are low-cost networks that measure $\text{PM}_{2.5}$, the mass concentration of fine particulate matter in the air. Additionally, there is one reference device with high quality measurement of $\text{PM}_{2.5}$. The reference device was moved to its current location at Lake Montebello in 2022, from its former location at Oldtown closer to the center of the city. A map of the networks is shown in Figure 1. Note that the networks have different geographic distributions, with the PurpleAir network being concentrated closer to the center and north of the city and having no sites in the southeast corner of the city. This indicates that there may be stronger preferential sampling in the PurpleAir network. Section 4.1 will explore this possibility further.

We wish to combine the information from the two LCS networks along with the data from the single reference device to make predictions of the spatial distribution of $\text{PM}_{2.5}$ in Baltimore. Since the two networks use different types of sensors, they may have different biases, and thus they cannot be treated as one larger network. Given the severe lack of spatially-resolved $\text{PM}_{2.5}$ data in Baltimore, we seek a model that offers unified predictions of $\text{PM}_{2.5}$ combining

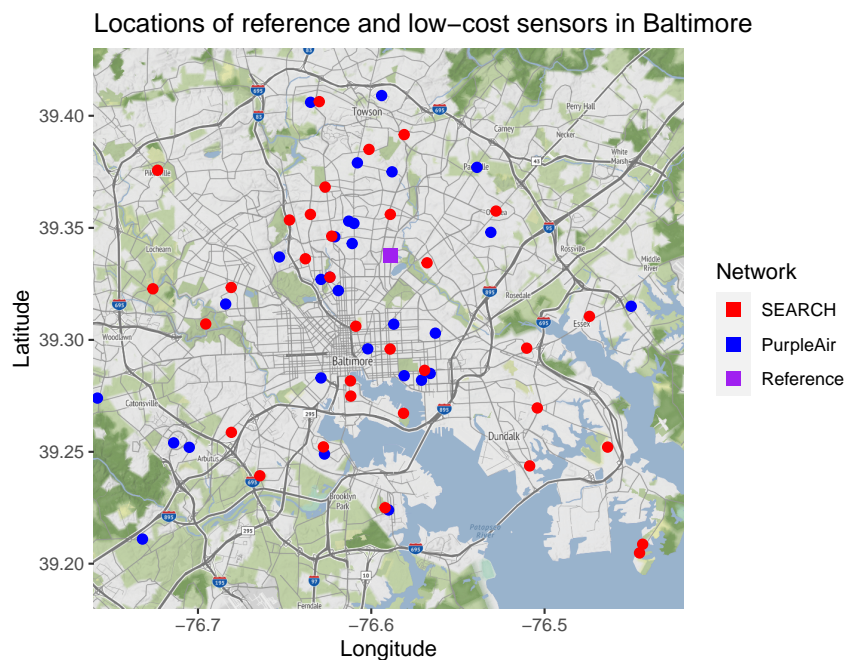


Figure 1: Low-cost sensor networks in Baltimore in 2023. The red sites are the SEARCH low-cost network. The blue sites are the PurpleAir low-cost network. The purple site is the reference device at Lake Montebello, which also has two SEARCH sensors at the same location.

data from these three sources. Contingent upon adequate model validation under different conditions, the model can then be used to make spatially-detailed map of air quality in Baltimore as new data is collected, which in turn can be used in downstream health association studies or policy evaluations to assess the burden of air quality in Baltimore.

For this study, we consider the period of June and July 2023, an unusual time for air quality in Baltimore because there were several days of extremely high $PM_{2.5}$ concentrations due to wildfire smoke, interspersed in days of typical concentrations. Heffernan et al. (2023) showed that the single-network spatial filtering method theoretically performs well at high concentrations, but there were only very limited days of poor air quality in the study period of Heffernan et al. (2023). It is important to check the performance of any low-cost sen-

sensor calibration method at such high concentrations, especially to assess impact of potential model misspecification as the training window for these models will not often include high concentrations. The chosen study period thus provides the unique opportunity to validate our proposed approach across a wider range of concentrations.

3 Methods

3.1 Overview of the single network GP Filter

We first briefly review the single network filtering approach, GP Filter, of Heffernan et al. (2023). This method considers a low-cost sensor (LCS) network and a sparse reference network (typically with one or very few sites). A schematic of such a low-cost network is shown in Figure 2 (left), with the purple sites being reference sites and the red sites being the low-cost network sites.

Heffernan et al. (2023) proposed the following two-stage model to combine data from the LCS network y and the reference devices x to predict the true concentrations across the region:

$$\begin{aligned} \text{Observation model: } y(\mathbf{s}, t) &= \beta_0 + \beta_1 x(\mathbf{s}, t) + \beta_2 \mathbf{z}(\mathbf{s}, t) + \beta_3 x(\mathbf{s}, t) \mathbf{z}(\mathbf{s}, t) + \epsilon(\mathbf{s}, t) \\ \text{State space model: } (\mathbf{x}(\mathbf{S}_0, t), \mathbf{x}(\mathbf{S}_1, t)) &\sim N(\mu_t, \mathbf{C}_t) \end{aligned} \tag{1}$$

where $x(\mathbf{s}, t)$ denotes the true pollutant concentrations as would be measured by a reference device at location \mathbf{s} and time t , $y(\mathbf{s}, t)$ denotes the measurement from the low-cost sensor, and $\mathbf{z}(\mathbf{s}, t)$ denotes other covariates (detailed later) that influences the bias of the low-cost data. The set of locations \mathbf{S}_0 are the locations with reference sites, the set of locations \mathbf{S}_1 denotes locations with low-cost devices but no reference device, $\mathbf{x}(\mathbf{S}_0, t)$ denotes $x(s, t)$ for

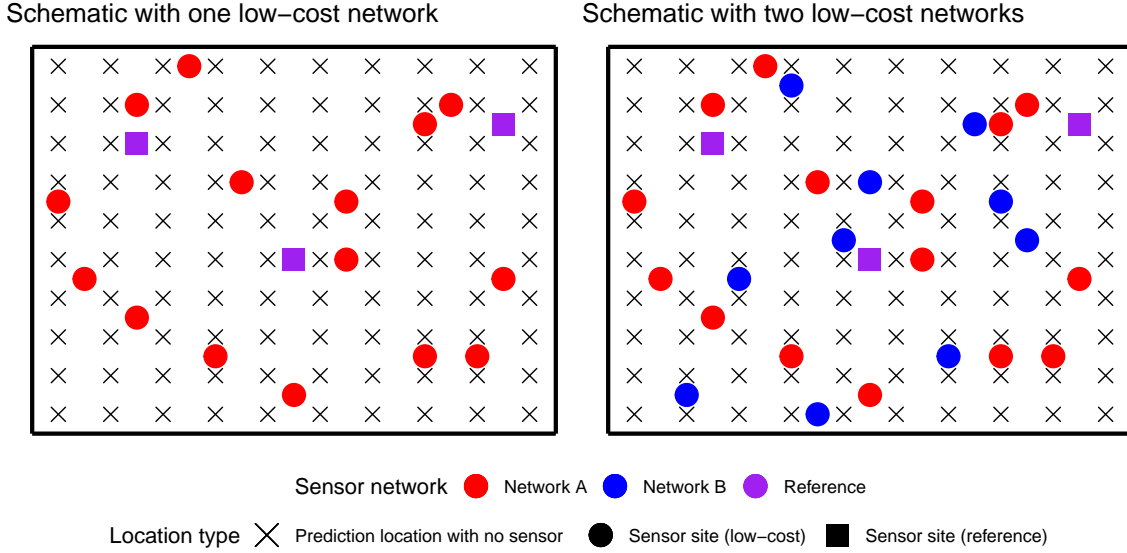


Figure 2: Illustrations of multiple networks operating in a same region: with (left) one or (right) two low-cost network(s) and 3 reference sites.

$s \in \mathbf{S}_0$ and other quantities are similarly defined. The state space model accounts for the spatial correlation in the true air pollution levels by assuming that the true air pollution surface $\mathbf{x}_t = \{x(\mathbf{s}, t), \forall \mathbf{s}\}$ follows a Gaussian Process $\mathbf{x}_t \sim GP(\mu_t, C_t)$, with time-specific mean μ_t and covariance function C_t . At a finite set of locations, the Gaussian Process is a multivariate normal distribution, as shown in the second equation of Equation (1), where the covariance between sites depends on the site locations and on covariance parameters. The observation model is a linear regression equation with errors $\epsilon(\mathbf{s}, t)$. Heffernan et al. (2023) modelled the errors as i.i.d with a Gaussian distribution. Note that at the reference sites (purple sites), we say that the true concentration x is observed, since the reference measurement is the gold standard for measurement, while at the low-cost sites, only y is observed and we wish to predict x . The observation model is a natural way to model data from low-cost sensors because the low-cost measurement is modelled as the noisy version of the true concentration x . The state space model assumes that air pollution concentrations

form an underlying smooth spatial surface, which is another realistic modelling choice.

The GP Filter presents several advantages over typical field-calibration approaches. First, the use of the observation model with x as the independent variable means that x is not systemically underestimated when it is large (Heffernan et al., 2023), which is a limitation of many regression-based calibration techniques that typically regress the true concentrations x on the low-cost data y . Additionally, we incorporate spatial information, both from other network sites and from available reference devices, into prediction, while common calibration approaches only use a particular site’s measurement for calibration.

The spatial filtering has two modules: i) training of the observation model, and ii) simultaneous training of the state-space model and spatial filtering. The parameters of the observation model, both the regression coefficients and the error model variance, are typically estimated before filtering is performed – as is common in Kalman-filtering or other filtering applications. For this, low-cost sensors are collocated with one or more of the reference sites permanently or for a long period of time. Then, the observation model can be trained on this abundant data, yielding highly precise estimates of the parameters which are subsequently held fixed at these estimated values for the filtering module. For particulate matter, it is typically assumed that the observation model trained from the collocated sensors can be applied to other sites in the network and has been empirically validated for the SEARCH low-cost sensors in Baltimore (Datta et al., 2020). However, we note that this same assumption would not be appropriate for gas sensors where the nature of the bias can be device-specific. For such a pollutant, one can still apply GP filter but would need device-specific observation models instead of network-specific ones as we use here. During the filtering part, the parameters of the state space model and the latent true concentrations are jointly estimated using the hierarchical model (1) in a Bayesian implementation. Priors are added to μ_t and the parameters of \mathbf{C}_t ,

and the parameters and $\mathbf{x}(\mathbf{S}_1, t)$ are estimated simultaneously using Markov Chain Monte Carlo (MCMC).

The Bayesian filtering formulation lends itself to the possibility of having multiple low-cost networks in a region, each with a different observation model, tied to the same state-space model for the true concentrations. Thus, data from multiple networks can be used together to make unified predictions both at the network sites and across the entire region. We present such an extension of the GP Filter, which we call the *Multi-network Gaussian Process Filter (MGPF)*, in Section 3.2. We discuss the benefits of combining multiple low-cost networks when they are available in Section 3.3.

3.2 Multinetwork Gaussian Process Filter

A schematic of a region with multiple low-cost sensor networks, such as Baltimore, is shown in Figure 2 (right). The first low-cost network (in red) is still present, but the second low-cost network (in blue) has now been added. Let A and B denote the two LCS networks, \mathbf{S}_A and \mathbf{S}_B denote the respective set of LCS locations for the networks, and \mathbf{S}_0 denote the reference network (only one site in Baltimore). We extend the model in (1) naturally to include two networks. Continuing to use the Gaussian Process $\mathbf{x}_t \sim GP(\mu_t, C_t)$ as the underlying air

pollution distribution, we can write the model as follows:

Observation model A: $\mathbf{y}(\mathbf{S}_A, t) =$

$$\beta_{A,0} + \beta_{A,1}\mathbf{x}(\mathbf{S}_A, t) + \beta_{A,2}\mathbf{z}(\mathbf{S}_A, t) + \beta_{A,3}\mathbf{x}(\mathbf{S}_A, t)\mathbf{z}(\mathbf{S}_A, t) + \epsilon_A(\mathbf{S}_A, t)$$

Observation model B: $\mathbf{y}(\mathbf{S}_B, t) =$

$$\beta_{B,0} + \beta_{B,1}\mathbf{x}(\mathbf{S}_B, t) + \beta_{B,2}\mathbf{z}(\mathbf{S}_B, t) + \beta_{B,3}\mathbf{x}(\mathbf{S}_B, t)\mathbf{z}(\mathbf{S}_B, t) + \epsilon_B(\mathbf{S}_B, t)$$

State space model: $(\mathbf{x}(\mathbf{S}_0, t), \mathbf{x}(\mathbf{S}_A, t), \mathbf{x}(\mathbf{S}_B, t)) \sim GP(\mu_t, \mathbf{C}_t)$

(2)

where ϵ_A and ϵ_B are independent errors. Rather than assuming i.i.d. errors as was done in Heffernan et al. (2023), we allow for heteroscedastic errors (details in Section 3.4). Our methodology can be used with any valid Gaussian process covariance function C_t . In our application in Baltimore, the exponential covariance function will be used. The means μ_t can also be modeled as a regression on land-use variables, if available. Here, we model them as time-specific constants due to the limited number of total locations with a measurement. We note that while we primarily focus on two LCS networks as is the setting for Baltimore, this model can be written more generally to include K networks:

K observation models: $\mathbf{y}(\mathbf{s}_k, t) =$

$$\beta_{k,0} + \beta_{k,1}\mathbf{x}(\mathbf{S}_k, t) + \beta_{k,2}\mathbf{z}(\mathbf{S}_k, t) + \beta_{k,3}\mathbf{x}(\mathbf{S}_k, t)\mathbf{z}(\mathbf{S}_k, t) + \epsilon_k(\mathbf{S}_k, t)$$

for $k \in \{1, \dots, K\}$

State space model: $(\mathbf{x}(\mathbf{S}_0, t), \mathbf{x}(\mathbf{S}_1, t), \dots, \mathbf{x}(\mathbf{S}_K, t)) \sim GP(\mu_t, \mathbf{C}_t)$

(3)

We refer to the model with two or more low-cost networks as the Multinetwork Gaussian

Process Filter (MGPF).

As with the single network GP Filter, we use a Gaussian Process as the state space model in the MGPF, to model the underlying smooth true air pollution concentration surface. This GP is flexible enough to capture different types of surfaces, that may be very flat at some timepoints and highly variable at others. The observation models are different for each network to allow for different biases and noise structures. We model y as a function of the true concentration x since it is natural to allow the low-cost measurement to be a noisy version of the truth.

In Equation (3), the only known quantities are the LCS data $\mathbf{y}(\mathbf{S}_1, t), \mathbf{y}(\mathbf{S}_2, t), \dots, \mathbf{y}(\mathbf{S}_K, t)$ at the respective network sites and the true concentrations $\mathbf{x}(\mathbf{S}_0, t)$ at a handful of reference sites \mathbf{S}_0 . The goal is to estimate the true concentrations $\mathbf{x}(\mathbf{s}, t)$ at each LCS location $\mathbf{s} \in \mathbf{S}_1 \cup \mathbf{S}_2 \cup \dots \cup \mathbf{S}_K$. As discussed earlier, the parameters of each observation model are pre-estimated (we discuss the details in the next Section) in the training part of the model, after which $\mathbf{x}(\mathbf{S}_1, t), \mathbf{x}(\mathbf{S}_2, t), \dots, \mathbf{x}(\mathbf{S}_K, t)$ can be estimated jointly with μ_t and the parameters of \mathbf{C}_t in a Bayesian filtering model. It should also be noted that both the GPF and the MGPF can easily handle missing data. When a low-cost site \mathbf{s} does not have a measurement at a timepoint t for any reason, that site can be excluded from the corresponding network set of sites \mathbf{S}_k for that timepoint with no impact to the method.

Since the Gaussian Process models a smooth surface of true air pollution concentrations over the entire region, we can also predict concentrations at locations that do not have any low-cost sensor (the crosses in Figure 2). We refer to these locations as \mathbf{S}_{new} and note that they can be added into the GP part of the model to give

$$(\mathbf{x}(\mathbf{S}_0, t), \mathbf{x}(\mathbf{S}_1, t), \dots, \mathbf{x}(\mathbf{S}_K, t), \mathbf{x}(\mathbf{S}_{new}, t)) \sim GP(\mu_t, \mathbf{C}_t) \quad (4)$$

Thus, in addition to estimating the true concentrations at all the network sites, we can make predictions at any location at the same time as we predict concentrations at the low-cost sites using the posterior distribution of the unknown true concentrations given the reference and low-cost data:

$$\begin{aligned}
& p(\mathbf{x}(\mathbf{S}_1, t), \dots, \mathbf{x}(\mathbf{S}_K, t), \mathbf{x}(\mathbf{S}_{new}, t) | \mathbf{x}(\mathbf{S}_0, t), \mathbf{y}(\mathbf{S}_1, t), \dots, \mathbf{y}(\mathbf{S}_K, t)) \\
&= p(\mathbf{x}(\mathbf{S}_{new}, t) | \mathbf{x}(\mathbf{S}_0, t), \mathbf{x}(\mathbf{S}_1, t), \dots, \mathbf{x}(\mathbf{S}_K, t)) \\
&\quad \times p(\mathbf{x}(\mathbf{S}_1, t), \dots, \mathbf{x}(\mathbf{S}_K, t) | \mathbf{x}(\mathbf{S}_0, t), \mathbf{y}(\mathbf{S}_1, t), \dots, \mathbf{y}(\mathbf{S}_K, t))
\end{aligned}$$

where the first term is a conditional normal distribution from a Gaussian process (i.e., the kriging predictive distribution), and the second term is the posterior distribution from the MGPF. So predictions can be obtained seamlessly after running the MCMC. These predictions, over a dense grid of locations, are used to create maps to inform spatial variability of the pollutant concentrations in the region.

3.3 Methodological benefits of the MGPF

The MGPF possesses numerous methodological benefits over existing calibration methods.

Dynamic calibration: In MGPF, both the calibration at the low-cost sites to estimate $x(\mathbf{S}_1, t), \dots, x(\mathbf{S}_K, t)$ and predictions at a new location $x(\mathbf{S}_{new}, t)$ are informed by the concurrent available latest data $x(\mathbf{S}_0, t)$, in addition to the low-cost data. The calibration is thus dynamic, informed by the latest reference data in the region. This is similar to the single network GP filter of Heffernan et al. (2023) but differs from the regression-based field calibration approaches which only use the reference data during the training of the regression coefficients, and do not use concurrent reference data when calibrating at a future time point.

Unified predictions and maps: MGPF offers a variety of qualities tailored to multiple low-cost sensor networks, that single-network calibration approaches applied individually to each network would not possess. MGPF creates unified predictions of air quality across a region with multiple measurement sources available. Individual calibration of each network by any method will result in different predictions with different uncertainties at each new location. Rather than having to choose an ad-hoc rule to combine predictions from different networks into a final prediction, MGPF will provide a single prediction with associated uncertainty for any location. Additionally, all the available data in the region (low-cost and reference) is used to inform predictions at all points, rather than only using a single network’s data to make the predictions at those network sites.

Robustness to preferential sampling: MGPF improves the accuracy of the predictions and robustness to preferential sampling, compared to the predictions using just 1 network. Using data from multiple networks can help better estimate the parameters of the state-space model for the true concentration (GP parameters μ_t and parameters of C_t), since low-cost measurements are made at more total locations. Additionally, as air pollution is spatially correlated, it is desirable to model all correlations – between locations of the same network, between two LCS networks, and between LCS networks and the reference data, as is done in our proposed MGPF. Predictions at locations that are somewhat isolated from sensors of one network but have proximal sensors from another network benefit from such joint modeling of the correlation of measurements across all networks. Accuracy may particularly be improved if there is preferential sampling in a network and predictions are being made at new sites \mathbf{S}_{new} . For example, a network with no sensors in the most polluted areas would not measure the highest concentrations in an area, and thus predictions across that area would likely be lower than the truth, (as we will see for the PurpleAir network in Section 4.1). This

is mitigated when one of the networks (in our case, the SEARCH network) do not suffer from preferential sampling. However, if all networks are preferentially sampled in an area, then even when all sites are combined, there can still be considerable bias in predictions at locations that do not have any sensor but have particularly high/low concentrations.

Improved uncertainty quantification: Finally, by synthesizing information from the denser combined set of locations, MGPF helps improve the uncertainty around predictions. Uncertainty around predictions can be decreased when multiple networks are used for similar reasons to the improved accuracy: combining data across networks, leads to measurements (low-cost or reference) from a denser set of sites that help decrease uncertainty. However, although on average, uncertainty decreases by using multiple networks, it is possible for two networks to measure conflicting concentrations at nearby sites. In this case, it is desirable for the multi-network filter to have larger uncertainty, since there is large variation in air quality in a small area. A single network in this case may be overconfident with its predictions.

As we will illustrate, these benefits of MGPF are manifested both at network sites and at locations in the region with no low-cost sensor.

3.4 Heteroscedastic observation models

The observation models are estimated before applying the spatial filtering for calibration and mapping. In some cases, such as the SEARCH network, at least one low-cost site is collocated with reference device(s) in the region. At the collocated sites, both x and y are measured, so the observation model can be trained using this data over a training window. If no sites are collocated within the region, such as for the PurpleAir network in Baltimore, then training the observation model is more complicated. Several possible ways to train

the observation model are to treat a reference and low-cost site that are close together as collocated, to identify days when there is little spatial variation for training using data from a remote reference site, or to train a model in a different region that has collocated sites from the same kind of device. Once the training data is selected, the observation model can be trained, and both the regression coefficients and the error model can be estimated.

Care must be taken to ensure that the model is well specified across the full range of concentrations that it will be applied to, including high concentrations. This can be challenging as typical concentrations in many major US cities are low on most days, leading to less amount of training data with high concentrations. Heffernan et al. (2023) proposed modeling the observation model noise as i.i.d. errors with homoscedastic variance. As we will see, at high concentrations, it is possible that the regression model remains correctly specified but that the errors $\epsilon(\mathbf{s}, t)$ are not i.i.d. As concentrations increase, the error variance also increases, implying heteroscedasticity which needs to be modeled. We consider a simple heteroscedastic model of the form:

$$\begin{aligned} \epsilon(\mathbf{s}, t) &\sim N(0, \tau^2) \\ \log(\tau^2) &= \alpha_0 + \alpha_1 \log(x(\mathbf{s}, t) + 1) \\ \text{or } \tau^2 &= \max(0, \alpha_0 + \alpha_1 x(\mathbf{s}, t)). \end{aligned} \tag{5}$$

where 1 is added to x because $\text{PM}_{2.5}$ is occasionally measured to be 0, but \log requires a strictly positive argument.

This model allows for sensors to have noise dependent on the true concentration, which, as we will see in the data analysis section, is a realistic depiction of how low-cost sensors work. Other models for the error variance portion of the observation model τ^2 should be considered

in different applications to select the most appropriate model form. Ideally, the regression model and the heteroscedasticity model could be trained on a previous period of time, and then be applied to the testing period. However, if the available training data does not cover the same range of true concentrations as the testing data, which is the case when applying the model to very high concentrations that the region has not witnessed in the recent past, it is reasonable to use the period where filtering will be performed to estimate the regression and/or heteroscedasticity component of the observation model.

4 Results: Calibrating Baltimore PM_{2.5} low-cost data

4.1 Preferential Sampling

From Figure 1, we notice that the PurpleAir network seems more geographically concentrated than the SEARCH network, lacking coverage especially in the southeast corner of the city. To investigate whether there is preferential sampling at play, we use a similar approach as Liang et al. (2021) to obtain location-specific estimated house prices and rents. We then look at the median and the range of prices and monthly rents across the two networks in Table 1. We see that PurpleAir sensors have a median price of \$53,500 more than the SEARCH sensors median price, and a median rent of \$332 more than SEARCH. Additionally, the ranges of both house prices and rents in the PurpleAir network are smaller than the respective SEARCH network ranges, indicating that the PurpleAir network does not capture the entire spectrum of house prices, and by extension all income levels, in Baltimore. The histograms of the prices and rents, as well as more details about how they are obtained, are shown in Supplement S1 and Figure S1. Figure S2 shows a histogram of the house prices in Baltimore according

to the American Community Survey (U.S. Census Bureau, 2024). The median house price is \$210,300, which is less than both the SEARCH and PurpleAir medians, but closer to the SEARCH median. Liang et al. (2021) also found that PurpleAir sensors tended to be in higher income areas. Therefore, preferential sampling may impact the predictions from the PurpleAir network.

Table 1: Median and range of house prices and monthly rents estimates at addresses near the network sensors.

		Network		Difference (PurpleAir - SEARCH)
		PurpleAir	SEARCH	
price (\$)	median	344,500	291,000	53,500
	max - min	691,300	767,400	-76,100
rent (\$)	median	2,500	2,168	332
	max - min	3,538	4,530	-992

4.2 Training observation models

There is only one reference device in Baltimore, at Lake Montebello. The SEARCH network has permanently installed two low-cost sensors that are collocated with the reference device. Thus we have ample collocated data to estimate the observation model parameters for the SEARCH network. We use 2 years of data, 2020-2021, to train the following observation model:

$$y(\mathbf{s}, t) = \beta_0 + \beta_1 x(\mathbf{s}, t) + \beta_2 \mathbf{z}(\mathbf{s}, t) + \beta_3 x(\mathbf{s}, t) \mathbf{z}(\mathbf{s}, t) + \epsilon(\mathbf{s}, t)$$

where \mathbf{z} is a vector of the covariates — relative humidity (RH), temperature (T) and a binary indicator for weekend (W). The SEARCH network has a lab-correction equation

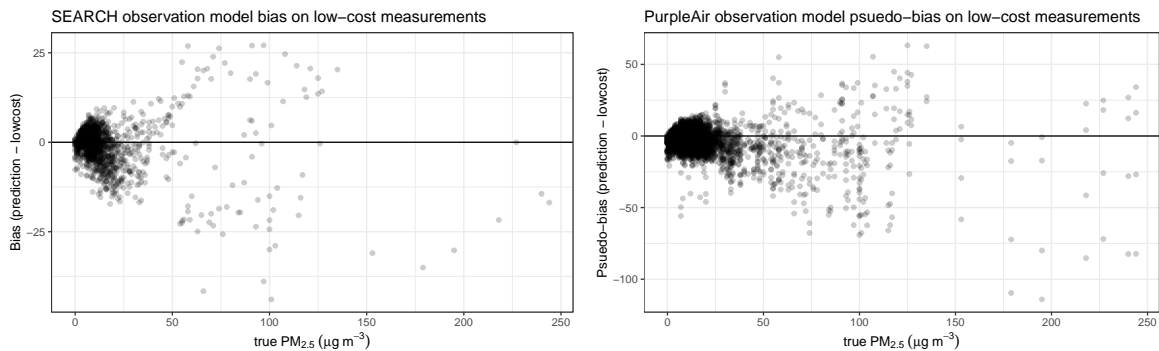


Figure 3: (Pseudo)-Bias of the (left) SEARCH or (right) PurpleAir observation model in June and July 2023 at the collocated Lake Montebello site (SEARCH) or the closest sites to the Lake Montebello site (PurpleAir)

(Levy Zamora et al., 2018), so we use the lab-corrected measurement as $y(\mathbf{s}, t)$.

During this two year training period of 2020-2021, the highest observed x is only $77 \mu\text{g}/\text{m}^3$, while in the testing period of June and July 2023, the highest x is $244 \mu\text{g}/\text{m}^3$. Therefore, care must be taken to ensure that the observation model is appropriate for the testing data. Figure 3 (left) shows the bias when this fitted observation model assuming homoscedastic errors is applied to predict the true concentrations at Lake Montebello during the out-of-sample time period of interest, June and July 2023. The bias is centered at 0, indicating that the estimated parameters for the regression part (mean) of the observation model do seem to be good fit for the higher concentrations. However, the error variance increases with the concentrations, thereby indicating the need for a heteroscedastic model.

We fit a heteroscedastic model for the observation model variance. We use the log model from Equation (5), i.e., $\log(\tau^2) = \alpha_0 + \alpha_1 \log(x(\mathbf{s}, t) + 1)$. We train the variance model on the period of June and July 2023 because the two-year training period used for estimating the regression coefficients do not have concentrations greater than $77 \mu\text{g}/\text{m}^3$, and extrapolating the variance model to higher concentrations may not be appropriate (see Section 5 and Figure S5 of Supplement S2) Once parameters of the the error variance model are estimated from

June-July 2023, we re-estimate the regression model coefficients by fitting a generalized least squares with these heteroscedastic errors ϵ using the 2020-2021 training data. This does not change the regression coefficients of the observation model very much, indicating again that the regression coefficients for the mean were well estimated, despite the variance being misspecified. We also considered fitting a model to the log concentrations but this model did not fit the data well (see Supplement S2, Figure S3).

For the PurpleAir network, we have no collocated devices in the entire region, and since the sensors used are different from the SEARCH sensors, we cannot assume that the same observation model holds for both networks. Several attempts to train an observation model using Baltimore data proved unsuccessful (see Supplement S2, Figure S4). Therefore, we instead use the US nationwide calibration equation for PurpleAir sensors (Barkjohn et al., 2021), which can be solved for $y(\mathbf{s}, t)$ to give

$$y(\mathbf{s}, t) = -10.97 + 1.91x(\mathbf{s}, t) + 0.16RH(\mathbf{s}, t) + \epsilon(\mathbf{s}, t). \quad (6)$$

This is the observation model we use for the PurpleAir network. Note that the SEARCH network observation model uses three covariates, RH, T, and W, while the nationwide calibration equation for PurpleAir found that only RH was needed as a covariate, showing how different sensors have different biases. Additionally, there is no interaction between RH and x in the PurpleAir observation model, while an interaction was found to be beneficial to the SEARCH observation model.

We see in Figure 3 (right) that the pseudo-bias (as the reference is not exactly collocated) for the PurpleAir sensors on the test data is roughly centered around 0, so the mean model in (6) is reasonable for the June and July 2023 data, but as with the SEARCH network, there

is evidence of heteroscedasticity. We use the June and July 2023 data to train the model for τ^2 , again using the log model from Equation (5), $\log(\tau^2) = \alpha_0 + \alpha_1 \log(x(\mathbf{s}, t) + 1)$. A comparison of training the variance models using data from June and July 2023 as opposed to June 2022 - May 2023 is shown in Supplement S2 Figure S5, revealing the need to train the variance model during the window with high concentrations (June and July 2023).

The fitted observation model variances, as well as a plot of the log squared bias which is the outcome in the fitted model we use, are shown in Figure S6. The fitted observation models (the regression coefficients for both the mean and the variance models for both networks) are shown in Table 2.

Table 2: Observation model parameters for SEARCH and PurpleAir networks

Term	SEARCH	PurpleAir
Intercept	-0.9756	-10.9733
true PM _{2.5}	1.0789	1.9084
RH	0.0422	0.1645
Temp	-0.0357	
weekend	0.4086	
true PM _{2.5} * RH	-0.0030	
true PM _{2.5} * Temp	0.0058	
true PM _{2.5} * weekend	-0.0736	
variance model intercept	-1.2136	0.4973
variance model slope	1.1774	0.8802

4.3 Prior specification

Subsequent to training the observation models, we apply the MGPF to filter hourly data. To stabilize the predictions and avoid very local fluctuations greatly impacting the GP covariance

structure, we use the following specification for our GP:

$$\begin{aligned}
 (\mathbf{x}(\mathbf{S}_0, t), \mathbf{x}(\mathbf{S}_A, t), \mathbf{x}(\mathbf{S}_B, t)) &\sim GP(\mu_t, \mathbf{C}_t) \\
 \mathbf{C}_t(d) &= \sigma_t^2 \exp\{-\phi_t d\} + \sigma_{n,t}^2 \mathbb{I}_{d=0}; \\
 \mu_t &\sim U(0, \infty); \quad \sigma_t^2 \sim U(0, s_{max}); \\
 \phi_t &\sim U(\phi_{min}, \phi_{max}); \quad \sigma_{n,t}^2 \sim U(0, s_{n,max})
 \end{aligned}$$

We use an exponential covariance structure with spatial variance σ_t^2 and spatial decay ϕ_t to model the spatial structure in the true pollutant concentrations. The nugget $\sigma_{n,t}^2$ is added to model micro-scale variations in PM_{2.5} levels. The upper bound on the nugget, $s_{n,max}$ is chosen to be the variance of the SEARCH lab-corrected data for that timepoint. This data has already gone through one round of correction, unlike the PurpleAir data, so it is on a more similar scale to the true concentrations. This bound essentially allows for all the data variance to be in the nugget, which is fairly generous, to allow for time-points where the spatial variability in concentrations will be very high. The bound on the spatial variance σ_t^2 is twice the variance of the predictions from the inverse model, again a generous bound. We allow for a larger bound of σ_t^2 than $\sigma_{n,t}^2$ because we believe that the spatial variance should generally be larger than the nugget variance at most timepoints when there is limited variability in air quality in the area. Finally, the range of the uniform prior for ϕ_t is selected so that the correlation at the farthest points in the network is between 2% and 98%. These bounds prevent the Bayesian sampler from going into extreme and unlikely parameter values, and ensure that there is at least some smoothness in air pollution concentrations.

4.4 Performance in June and July 2023

We now present the results of applying the MGPF to the SEARCH and PurpleAir networks. There are three main periods during June and July 2023 where concentrations were elevated: June 7-8, June 28-30, and July 17-18, with concentrations going up to almost $250 \mu\text{g}/\text{m}^3$. The distribution and time series of true concentrations are given in Table S1 and Figure S7. At every hour, we perform filtering using only the PurpleAir network, only the SEARCH network, and using both networks. One important metric to understand the impact of multi-network filtering is to assess the difference in uncertainty. We will calculate a percent difference in the length of the confidence interval (CI) using two networks (l_2) compared to one network (l_1):

$$\%diff = \frac{l_2 - l_1}{l_1} * 100 \quad (7)$$

We compare the predicted concentrations and the length of CIs at network sites when both networks are used to when only that network is used in the filtering (Figure 4, top left and bottom left). We see the percent differences in CI lengths averaged by monitor (top left) and by timepoint (bottom left) at the network sites. We see decreases in CI length when two networks are used compared to using a single network for every monitor. The decrease is bigger at the SEARCH network sites when PurpleAir is also used for filtering, than when it is the other way around. There are 83% of hours with a decrease in CI length using two networks, and the median change in CI length across the network is -9.49% . Many, but not all, of the timepoints where uncertainty increases correspond to the periods with higher concentrations (purple time series), showing that an individual network may be overconfident

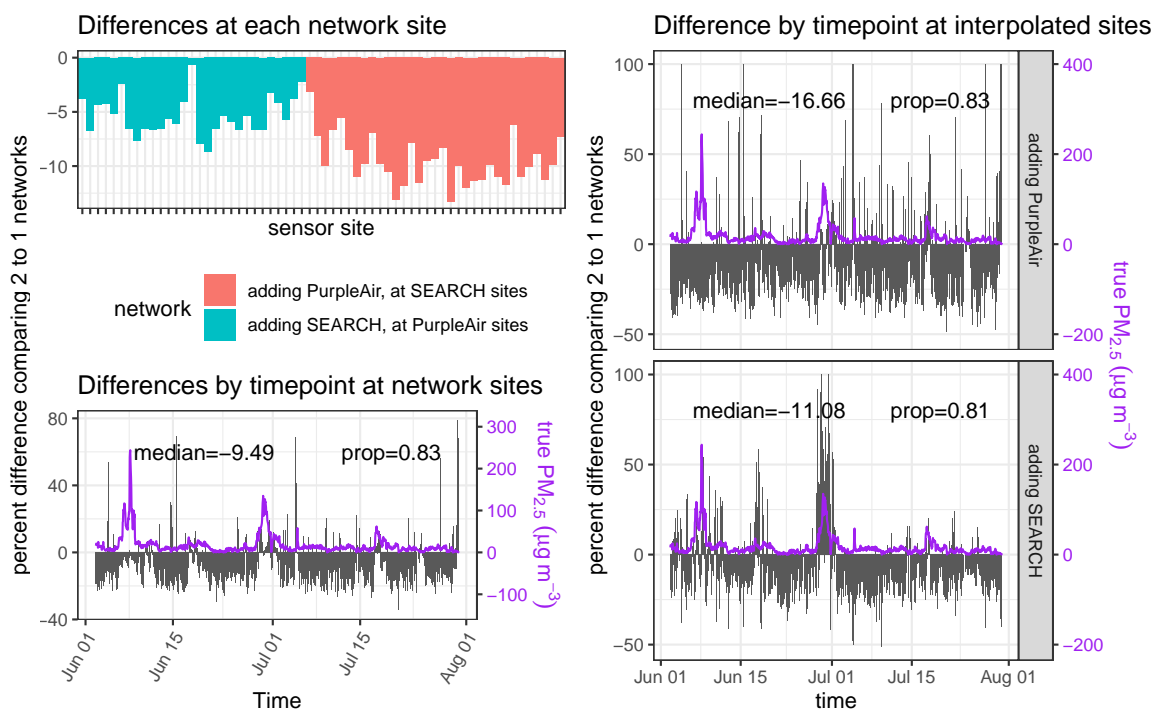


Figure 4: (Top left) Percent difference in CI lengths, for each monitor from the PurpleAir and SEARCH networks, averaged across time. (Bottom left) Percent difference in CI lengths, for each timepoint, averaged across the PurpleAir and SEARCH networks. (Right) Percent difference in CI lengths averaged across all interpolated sites in Baltimore, using both networks compared to using only one network, capped at 100%. The median of the percent differences, and the proportion p of percent differences that are negative, are listed. The purple lines are the true concentrations at the reference site at Lake Montebello.

when concentrations are high. Some diagnostics of applying the method on this dataset, such as a looking at the spatial parameter estimates and a comparison of the MGPF predictions and predictions from the observation model alone, are shown in Supplement S3.

We also make predictions of $PM_{2.5}$ across Baltimore, on a fine grid of locations, and plot in Figures 4 (top right and bottom right), for each network, the time-series of average change in uncertainty when adding the second network. We see that the CI length when using two networks is smaller than when using one network 81 – 83% of the time. The median percent change in CI length across the city using the multi-network GP filter is -17% compared to

filtering using the SEARCH network, and -11% compared to filtering using the PurpleAir network. We also see that for a few timepoints, the CIs from MGPF can increase in length by over 100% . This is usually because one network (often the PurpleAir network) is overconfident and has very narrow intervals when used alone. This tends to happen when the PurpleAir predicted surface is very flat (Supplement S3, Figure S8). The percent decreases at interpolated sites are larger than at the network sites, showing that the biggest advantage of using two networks is in making predictions at new locations. The absolute difference in CI lengths at network sites and interpolated locations are shown in Figures S9 and S10. Additional model validation is shown in Figures S11 and S12.

Additionally, we look at maps of concentrations overall during this two month period. The mean of the predictions at the interpolated sites is shown in Figure 5 for high pollution days (top), i.e., the days with the top 10% of concentrations measured by the reference sensor at Lake Montebello, and on the remaining days which are more representative of typical concentrations in Baltimore (bottom). There are clear differences between the predictions from different methods. In particular, in the southeast portion of the city, the PurpleAir network has lower predicted concentrations. This is due to the preferential sampling in the PurpleAir network, having no sensors to measure the higher concentrations in that part of the city. PurpleAir estimates a flatter surface on average, while SEARCH and the two networks combined have more variability across the city.

Figure 6 shows the average length of CIs across the two months. We see different behaviors for high and non-high timepoints. For high timepoints, SEARCH benefits most from uncertainty reduction by adding PurpleAir, while the PurpleAir intervals can be overly conservative. For non-high timepoints, SEARCH and PurpleAir alone have comparable lengths, and both networks benefit greatly from adding the other network. From this, we see that

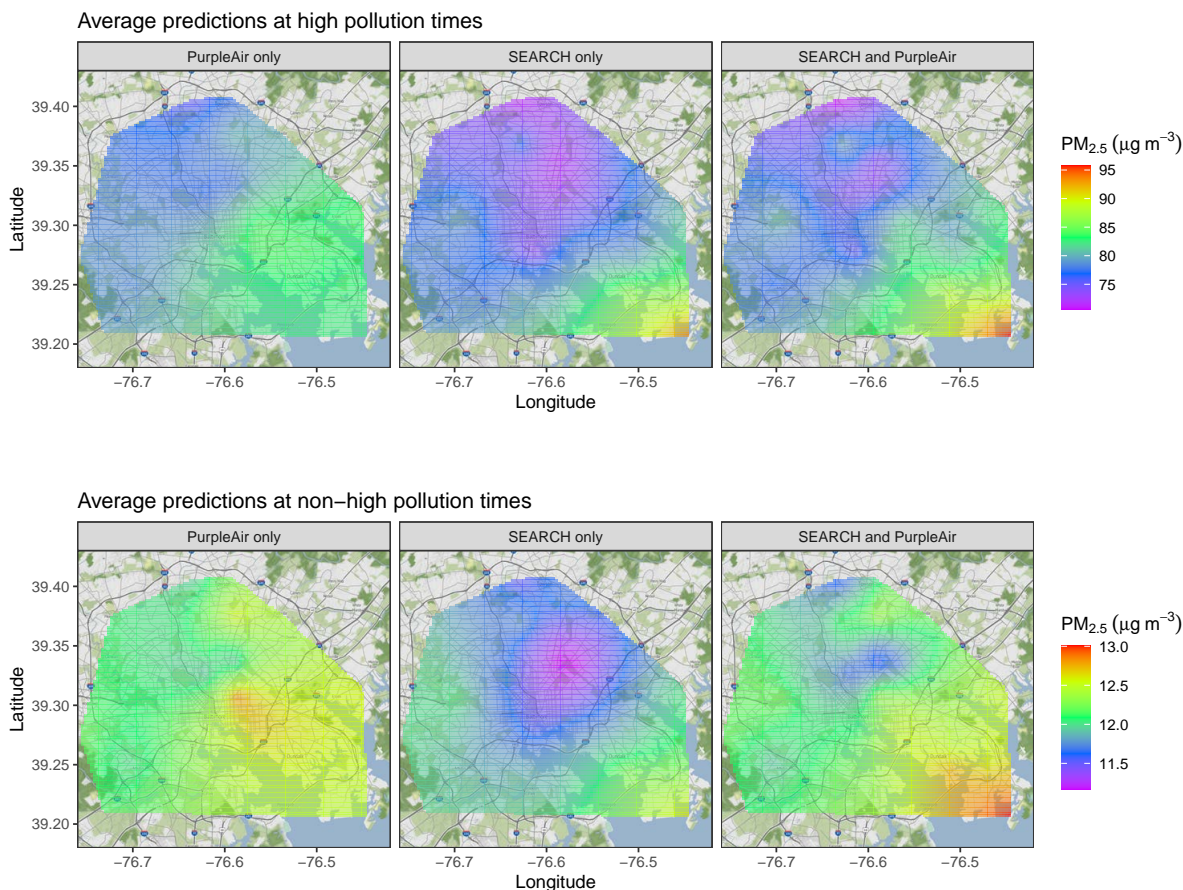


Figure 5: Mean of predicted PM_{2.5} in Baltimore (Top) over the days with high pollution (Bottom) over all remaining days.

there are benefits in terms of prediction accuracy (especially in the PurpleAir network) and in uncertainty (especially in the SEARCH network) from using a multi-network approach to filtering. Figures 5-6 don't show the network sites for clarity of presentation. The figures including the network sites are in Figures S13-S14. We also present maps of the average concentration and CI length over the entire two-month period, as well as an example of a map for a single timepoint and a comparison of CI lengths in certain periods, in Supplement S3 (Figures S15-S18).

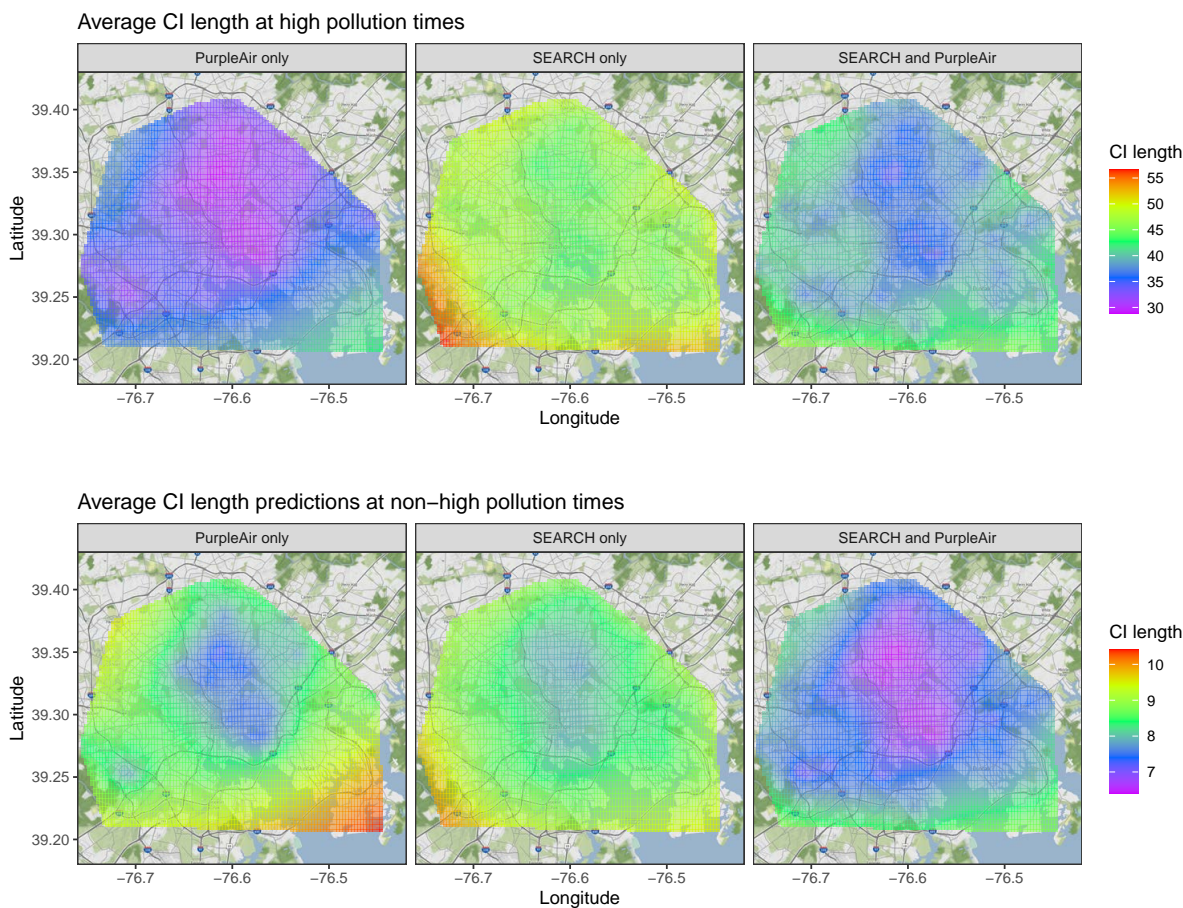


Figure 6: Average confidence interval length of predicted $\text{PM}_{2.5}$ in Baltimore (Top) over the days with high pollution (Bottom) over all remaining days.

Another approach to combine data from multiple networks is to individually calibrate each network using a linear regression calibration equation, and then to interpolate using inverse distance weighting (IDW) (Mueller et al., 2004). This approach does not model spatial correlation across different locations, which leads to an interpolated surface with much more fluctuation on average, especially around network sites (Figures S19, S20), and it suffers from underestimation (Figure S21). The pseudo-RMSE of the IDW method is also higher than the MGPF (Figure S22). More details are given in Supplement S3.

5 Results: Simulation studies

We also perform simulation experiments to validate the performance of MGPF.

5.1 Filtering results

We aim to illustrate the better accuracy, lower bias, and lower uncertainty of the MGPF with two networks compared to using either network individually. We simulate data as follows: we sample 30 sites for each network and 1 reference site from a unit square. The reference site is sampled near the center of the square, and the network sites are sampled either randomly or with preferential sampling. If there is preferential sampling, we randomly sample 20% of the sites from the full unit square, and the remaining 80% of the sites from a smaller square within the unit square. To simulate true concentrations, we sample from a Gaussian Process with a small mean μ_t to represent a low level of ambient concentrations. We also create two point sources, which are located in the area where the preferentially sampled network will have fewer sensors. These point sources each have a randomly sampled concentration they emit, with locations closer to the source having more pollution from that source. This means that concentrations in the area that is not preferentially sampled are higher on average than in the area that has preferential sampling. We sample 10 datasets, each with 100 timepoints. More details about the simulation setup and data generation are included in Supplement S4. Given the true concentrations, we simulate relative humidity, and generate a low-cost measurement from an observation model. The first low-cost network observation model regression coefficients are the PurpleAir coefficients. For the second observation model, we use an observation model whose regression coefficients and variance are both proportional to the first

observation model. This way, the amount of uncertainty in each network scales with the magnitudes of the observations from that network. The observation models equations are included in Supplement S4.

In Figure 7, we show the percent difference in CI lengths using two networks compared to one network, where we use Equation (7) to calculate the percent difference. On the top left, we see a benefit of using both networks when it comes to uncertainty reductions at network sites, with uncertainty going down by 6-7% on average. There is little difference in the CI reductions between networks, or comparing random and preferential site sampling. Looking at CI length across the whole sampling region (top right), we see much larger reductions everywhere, just over 30%. Again there is little difference between networks.

We also look at the bias and RMSE of the method, at all interpolated locations in the network (bottom of Figure 7). We see that when the sites are randomly sampled, bias is fairly low. However, under preferential sampling, filtering only using Network B, which was preferentially sampled, results in a large negative bias. Filtering using the two networks together results in substantially less bias than filtering only using Network B. For RMSE, under preferential sampling, Network B also has much larger RMSE than Network A. Overall, using both networks results in smaller RMSE than either network individually, both under random and preferential sampling.

This set of simulations demonstrates that the MGPF can indeed accomplish the goals that were outlined in Section 3.3. A unified set of predictions across the region was made, and these predictions had better accuracy (lower RMSE) and better uncertainty (lower CI length) than using either network individually. Additionally, we demonstrated that in the case of preferential sampling, as we see in the PurpleAir network, there can be systematic bias when areas with more extreme concentrations are more/less sampled, which is mitigated in the

multi-network filtering.

5.2 Observation model considerations

In the previous simulations, we assumed that the training data had the same distribution as the test data. However, in practice, the training dataset may not cover the full range of the testing data, so we investigate the impact of training on a smaller range in this simulation. Since each observation model gets trained independently, it is enough to consider one network to illustrate the potential issues with training an observation model. We generate data using the PurpleAir observation model regression coefficients, with the observation model variance being a linear function of the true concentrations x . We generate 2,000 training timepoints and 100 testing timepoints. We consider two cases: first, the range of the training data is the same as the range of the testing data. Second, the range of the training data is 1/3 the range of the testing data, with no high concentrations. This is similar to what we see in the case study. We fit the regression part of the observation model in both cases, and make predictions of the true concentrations from this observation model to see whether the point estimates from the model are correct. We also train the heteroscedastic variance model, and compare the resulting fit to the true heteroscedastic model.

Figure 8 (top) shows that the test RMSE of the observation model does not change much when training on the full range or a smaller range. This is still the case when only calculating the RMSE of higher concentration timepoints, which the smaller training data range does not cover. Thus, the regression coefficients are well estimated in both cases. However, we see from the bottom figure that the τ^2 estimates at a high concentration are considerably closer to the truth (the blue line) when the training data has the full range. Using a smaller

range, the τ^2 estimates are considerably larger than the true variance. This indicates that the heteroscedastic model training suffers when the range of the training data is too small, informing our decision to train the SEARCH observation model variance based on June and July 2023 data.

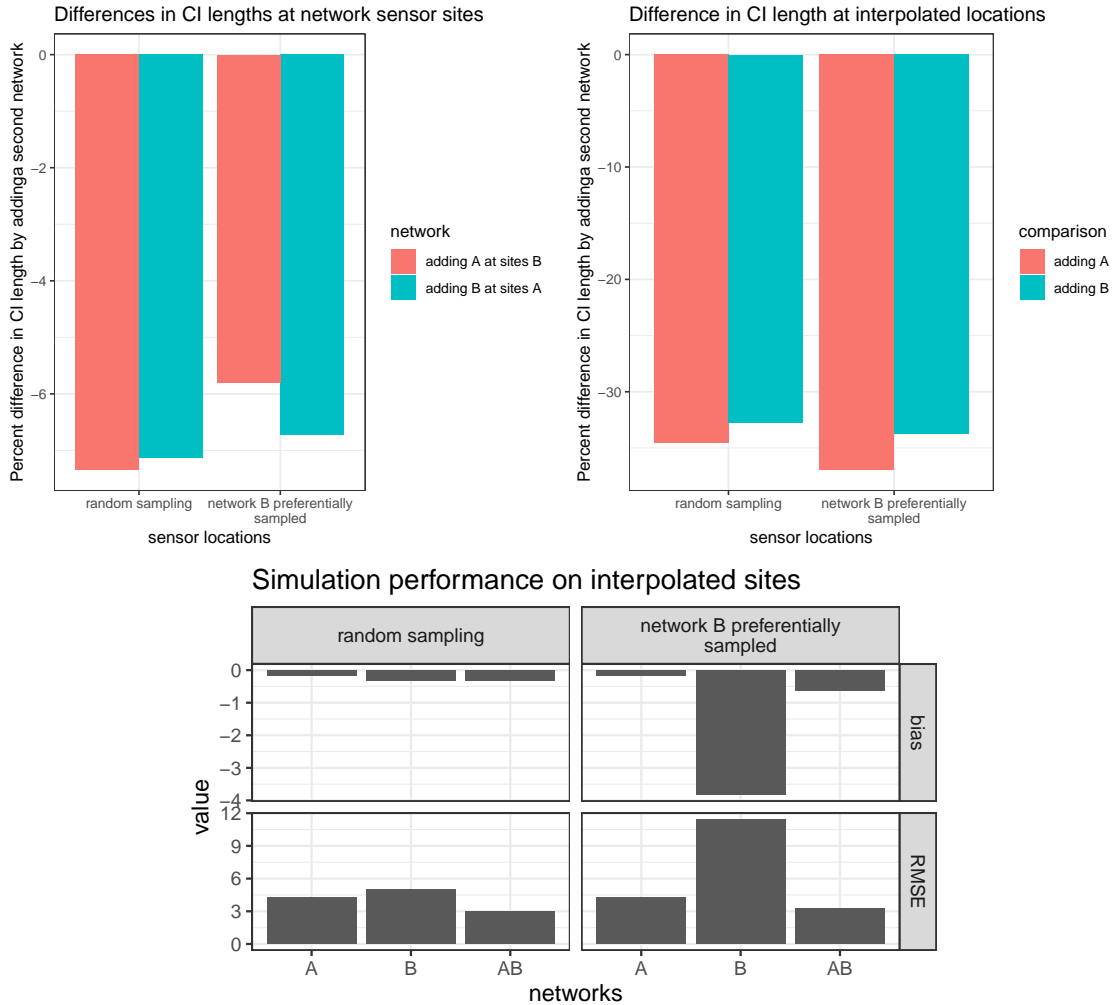


Figure 7: (Top left) Percent difference in CI lengths using 2 networks or 1 network, at device sites. (Top right) Percent difference in CI lengths across all interpolated locations in the sampling region. (Bottom) RMSE and bias across all interpolated locations in the sampling region.

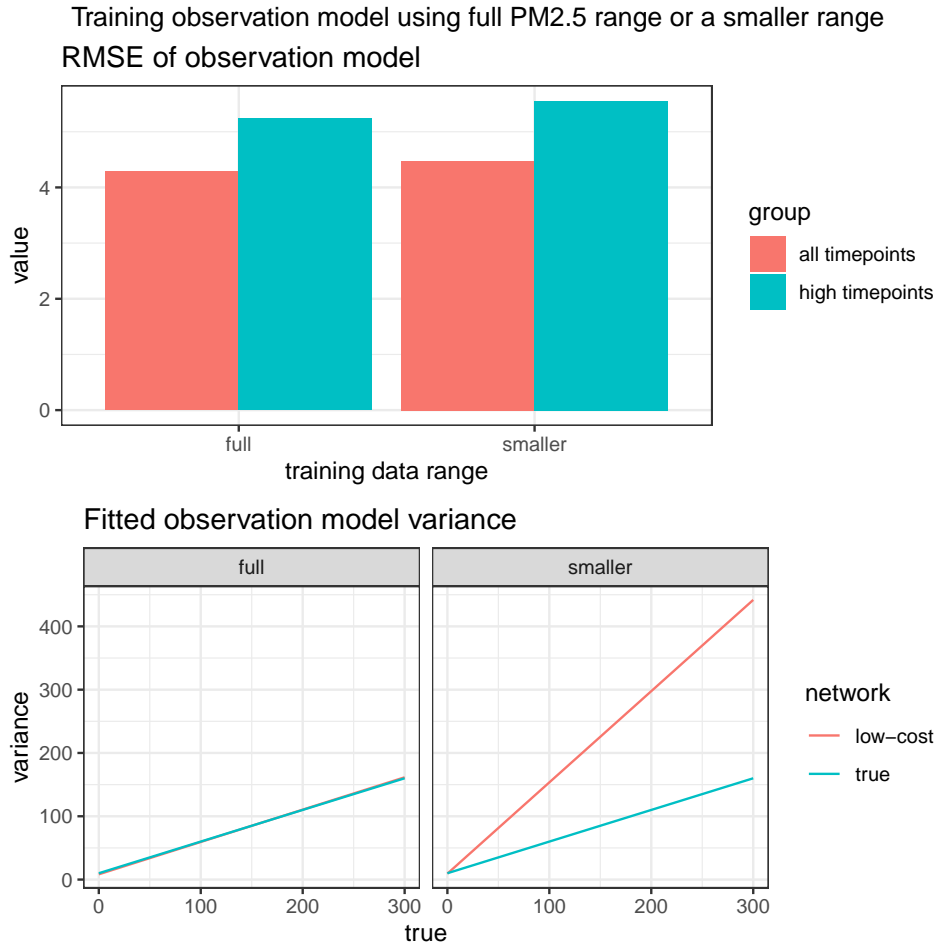


Figure 8: RMSE of predictions from inverting the observation model regression equation and predicting on test data, and estimate of the low-cost data observation model error variance (τ^2) model. The x-axis of the top graph and facets of the bottom panel show whether the training data had the full range of the testing data, or a smaller range. In the bottom left panel, the two lines are almost overlapping and thus the red line is not visible.

6 Conclusions

We have presented a new method, the MGPF, to calibrate data from multiple low-cost sensor (LCS) networks, each with different biases and noise levels, as well as an application of this method to combine $\text{PM}_{2.5}$ data from the SEARCH and the PurpleAir LCS networks, in Baltimore, Maryland. Regression equations have been published that calibrate the PurpleAir (Barkjohn et al., 2021) and SEARCH (Datta et al., 2020) networks, but using these equations in isolation means that spatial patterns are ignored. Since the spatial filtering approach that was developed for calibrating a low-cost network (Heffernan et al., 2023) is a Bayesian hierarchical model that models the low-cost measurement as a function of the true concentration, extending this methodology to include multiple networks with multiple unique observation models was natural. The spatial model allows for smoothing over space where appropriate, especially where the two networks have sensors very close to each other. Other potential approaches to combine data from two networks exist. One is to use spatial filtering to calibrate the low-cost measurements from each site individually to make predictions, with uncertainty, throughout the network, and then take an average, weighted or unweighted, of these predictions at each location as the final prediction. This approach provides uncertainty quantification for the final prediction, but could still be biased by the preferentially sampled network which is part of the average. Alternatively, estimates at sensor sites can be made for each network individually, and then inverse distance weighting (IDW) (Mueller et al., 2004) can be used to interpolate the predictions across the network (Supplement S3). This approach is likely to create large local fluctuations in predicted concentrations where the two networks have sites nearby, and IDW does not have associated uncertainty quantification. Additionally, when calibrating the networks individually and then combining, there

are many decisions that have to be made, such as whether to interpolate using each network and then combine or combine point estimates and then interpolate, whether and how to weight observations, and what weight to use in IDW. The MGPF simplifies these decisions by incorporating the calibration and interpolation steps into one, and using all data to do both of these steps.

Our approach is similar to Zimmerman and Holland (2005) and Fuentes and Raftery (2005), both of which model two networks with two different measurement models in the context of different applications. Our model is similar to an extension of this, where there are three networks instead of two, with the reference site(s) forming the third network with perfect calibration. In the case of Baltimore, this third network would consist of only one site. Zimmerman and Holland (2005) model a constant measurement bias, and they cannot identify that bias. Thus, they focus on predicting observations made from each of the networks. We focus on a context where one network is assumed to have no bias, and our problem of interest is to predict the outcome with no bias or noise, and we allow for non-constant bias. We further tailored our method to the problem of low-cost sensors in Baltimore, by focusing on the issues of heteroscedastic measurement error, preferential sampling, and calibration of high concentrations in a setting with a few high-quality sensors and some low-cost sites that are collocated with these high-quality devices.

The MGPF allows us to make unified predictions of air quality throughout the entire network using all data sources. These predictions leverage the Gaussian Process spatial state-space model for the true concentrations in the filtering and have their own associated uncertainty, which incorporates the uncertainty of the predictions at the sites themselves, unlike other interpolation approaches such as IDW that do not have coherent uncertainty quantification. The MGPF provides more trustworthy city-wide interpolated predictions compared to either

network individually, especially when preferential sampling is present, like in the PurpleAir network (Figures 5, 7). Uncertainty was also predominantly reduced, both in Baltimore (Figure 6) and in simulation (Figure 7). The uncertainty in the maps produced by MGPF can be used to identify areas with higher uncertainty, where adding a network site can be most beneficial.

Maps produced from MGPF can be used to answer environmental justice questions in Baltimore. The map in Figure 5 shows that higher concentrations seem to be observed in the south and southwest of the city. This means that these specific regions may be experiencing concentrations that exceed the EPA standards, especially now that the EPA’s annual standard is $9 \mu\text{g}/\text{m}^3$. More investigation is needed to determine which areas routinely experience air quality that exceeds EPA standards. There is evidence that there are environmental justice issues in the United States and Canada (Miranda et al., 2011; Anderson et al., 2018; Jerrett et al., 2001). Therefore, it is important to assess where such disparities could exist in Baltimore. Also, while we focus on $\text{PM}_{2.5}$ in this manuscript, the MGPF could be extended to other pollutants. Assuming the same observation model for an entire network, as we did in this work, is not possible for gas sensors, so alternative approaches to create sensor-specific observation models would be needed.

One future extension of the current method that could help address environmental justice concerns is to include a third network in our MGPF for Baltimore. In Curtis Bay, a neighborhood in south Baltimore with many sources of pollution, a group of researchers and residents are working to measure different types of pollution, including $\text{PM}_{2.5}$ (Aubourg et al., 2023). SEARCH and PurpleAir each have one monitor in this area, and Figure 5 shows that Curtis Bay has higher concentrations than most of the city. Including this network in the MGPF could improve the predictions in Curtis Bay.

The two-network MGPF filtering approach can be used as the new standard for calibrating low-cost data in Baltimore and interpolating predictions throughout the city. The gains in prediction accuracy and uncertainty quantification were clearly demonstrated in June and July 2023, thus the approach has proved itself able to filter high concentrations. Baltimore very infrequently experiences concentrations greater than $250 \mu\text{g}/\text{m}^3$, so the observation model regression coefficients and heteroscedastic model variance that we trained should be usable for the foreseeable future in Baltimore. Thus, the MGPF is a better choice to predict air quality in Baltimore compared to filtering either network individually.

Acknowledgement

This work was supported by the U.S. Environmental Protection Agency (Assistance Agreement no. RD835871 to Yale University); the Bloomberg American Health Initiative at the Johns Hopkins Bloomberg School of Public Health in collaboration with Alliance for a Healthier World at Johns Hopkins University; the Johns Hopkins University Data Science and AI Institute Demonstration Project Award (AD and KK); National Science Foundation Graduate Research Fellowship Program (grant No. DGE2139757 to C.H.); National Institute of Environmental Health Sciences (NIEHS) (grant R01 ES033739 to A.D., R.P. K.K., and C.H.). The authors declare they have nothing to disclose. The authors acknowledge Dr. Misti Levy-Zamora, Dr. Colby Buehler and Mr. Hao Lei for processing of the SEARCH data.

Supplement

S1 Zillow house prices and rents

We follow the approach of Liang et al. (2021) in understanding the extent of preferential sampling in the two low-cost PM_{2.5} networks in Baltimore. We input the co-ordinates of the sensors into Google Maps, and identify the closest house to each address. Then, we use Zillow.com, a housing website that provides estimates of the prices of many homes, to obtain an estimated price of that nearest house and the cost to rent the house, which are shown in Figure S1.



Figure S1: Histogram of the house prices and rents in Baltimore at the locations of the PurpleAir and SEARCH networks.

Figure S2 shows house prices according to the American Community Survey. Most of the houses fall in the \$200,000-\$300,000 range. Compared to SEARCH, the PurpleAir network

has fewer sensors next to homes worth less than the median of \$210,300 (Figure S1), showing that SEARCH better matches the demographics of the city, though still with a tendency towards locations where house prices are higher.

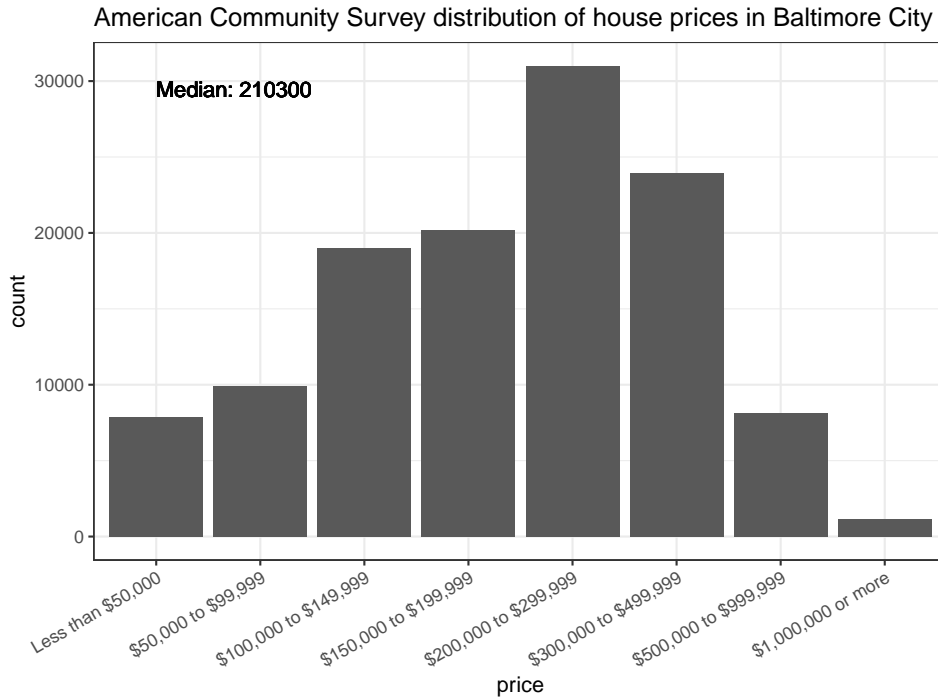


Figure S2: Histogram of the house prices in Baltimore City according to the American Community Survey.

S2 Training heteroscedastic models

Table S1 shows the distribution of the true concentrations across the training period for the SEARCH network (2020-2021) and the testing period of June and July 2023. We see that the concentrations are overall considerably higher in the testing period, and that the concentrations are more variable.

Since the bias in Figure 3 show evidence of heteroscedasticity, one approach to fitting the

Table S1: Summary statistics of true concentrations measured by the reference site in the training period for the mean part of the observation model (2020-2021) and the testing period (June and July 2023).

dataset	mean	sd	min	Q1	median	Q3	max
test	17.39	24.08	0	6	10	18	244
train	7.01	5.67	0	3	6	9	77

observation model is to model the log concentrations, $\log(y(\mathbf{s}, t) + 1) = \beta_0 + \beta_1 x(\mathbf{s}, t) + \beta_2 \mathbf{z}(\mathbf{s}, t) + \beta_3 x(\mathbf{s}, t) \mathbf{z}(\mathbf{s}, t) + \epsilon(\mathbf{s}, t)$ (where the +1 is needed since the measurements can be 0). We fit this model on the SEARCH data in 2020-2021, but we see in Figure S3 that the bias when this model is applied to June and July 2023 is very large as concentrations increase. Thus, a log model is completely inadequate for this data. Additionally, for the PurpleAir network, retraining a model on the log scale would be difficult due to the lack of collocation, as we discuss next, so we do not attempt to fit this model.

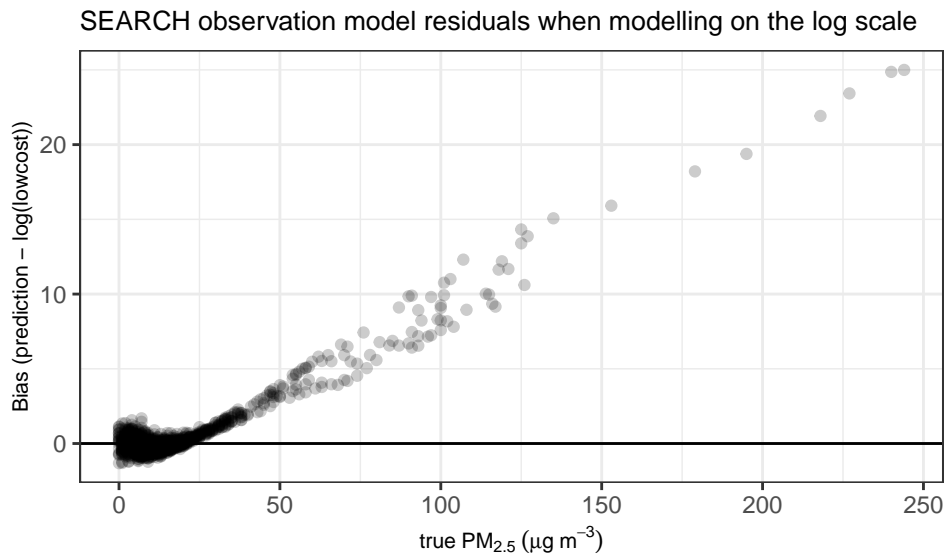


Figure S3: Bias from training the SEARCH observation model on the log scale.

We present an attempt to retrain the PurpleAir observation model regression coefficients, using one year of past data. Since we do not have collocated sites, we must assume that

the Lake Montebello true concentrations are equal to the true concentrations for some other time/site combinations. From this, a model can be fit. We present two ways of selecting the sites/times to use for training

1. using the timepoints where there was the least variation in the raw measurements from the PurpleAir sites. At these times, air quality can be assumed to be roughly similar across the city, and the reference data at Lake Montebello can be taken as a crude proxy for collocated reference. The 20% of timepoints with the smallest relative range are considered here, and all sites at these timepoints are used.
2. using the sites that are closest to Lake Montebello, and assuming the true concentration there is the same as Lake Montebello at all times. Thus, only four sites are selected, but all timepoints from the year are used.

The bias of the predictions from fitting the observation model using these approaches are shown in Figure S4. We see that there is a strong negative bias when training on the low variance timepoints, and a slightly smaller bias when using the nearby sensors, that is most visible for concentrations above $\sim 50\mu\text{g}/\text{m}^3$. Other approaches to select a training period or low-variance timepoints also resulted in similar types of negative biases. Since these biases are more extreme than what is observed in Figure 3 (right), which uses the Barkjohn et al. (2021) PurpleAir calibration equation (Equation (6)), we choose to use Equation (6) as our final observation model regression coefficients.

We also present a comparison of training the heteroscedastic part of the observation model using different time periods. For the SEARCH network, since we train the observation model regression coefficients using 2020-2021 data, it is natural to train the heteroscedastic variance model using the same time period. However, in Figure S5 we see that the estimated observa-

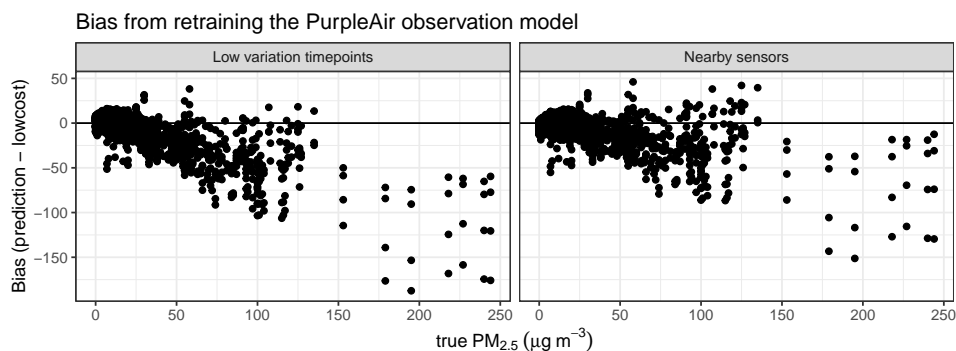


Figure S4: Bias from retraining the PurpleAir observation model using one year of past data.

tion model variance is very different using 2020-2021 (labelled “previous training window”), and June-July 2023 to train this part of the model. In both cases, the heteroscedastic model is trained on the square of the pseudo-bias obtained from the SEARCH observation model coefficients trained on 2020-2021 (from Figure 3). In particular, using 2020-2021, where the highest concentration was $77 \mu\text{g}/\text{m}^3$, requires extrapolation to estimate the variance at higher concentrations, and the big difference in variance from extrapolation and from training on a wider range illustrates that the extrapolated variances are likely less reliable.

PurpleAir data, using Equation (6) as the regression model, also has evidence of heteroscedasticity. Since no collocated data is available, we use the four closest sites to Lake Montebello as approximately collocated. We compare using June and July 2023 to train the heteroscedastic model to using the previous year of data, from June 2022 - May 2023. Figure S5 shows that when the previous year of data is used, the estimated heteroscedastic variance only goes up to about 25. This is completely outside of the range of other model fits, and a look at the out-of-sample bias in Figure 3 (right) shows that this estimate does not match what is observed in 2023. This example illustrates the dramatic error in extrapolation that can occur when fitting the observation model (in particular, the variance model) on data that does not cover the same range as the testing data. We also demonstrated via a simulation study in

Section 5.2.

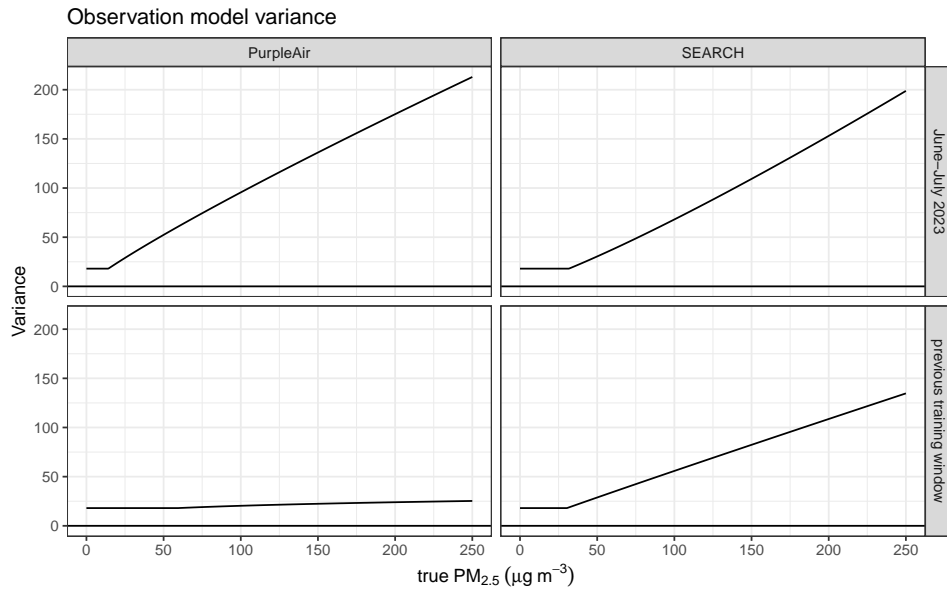


Figure S5: Estimated variance τ^2 as a function of the true concentration x , using different windows to train the variance model. For PurpleAir, the previous training window is June 2022-May 2023. For SEARCH, the previous training window is 2020-2021.

From these results, we conclude that using training data with considerably reduced variability in air pollution levels to estimate the observation model variances seems to lead to faulty extrapolation, especially in the PurpleAir data. Therefore, we use the June and July 2023 data to estimate this variance. Figure S6 (top) shows these variances once again, which are the variances from the top row of Figure S5. In Figure S6 (bottom), we see the log squared bias plotted against the log-true $\text{PM}_{2.5}$, which illustrates that the selected variance model is a reasonable fit to the error. To ensure that the variances do not become unrealistically small, which would result in the filtering putting considerable weight on the low-cost measurement and little weight on spatial information, we impose a minimum value for the variance, which is the naive τ^2 estimate from fitting the ordinary linear regression model on the 2020-2021 SEARCH data.

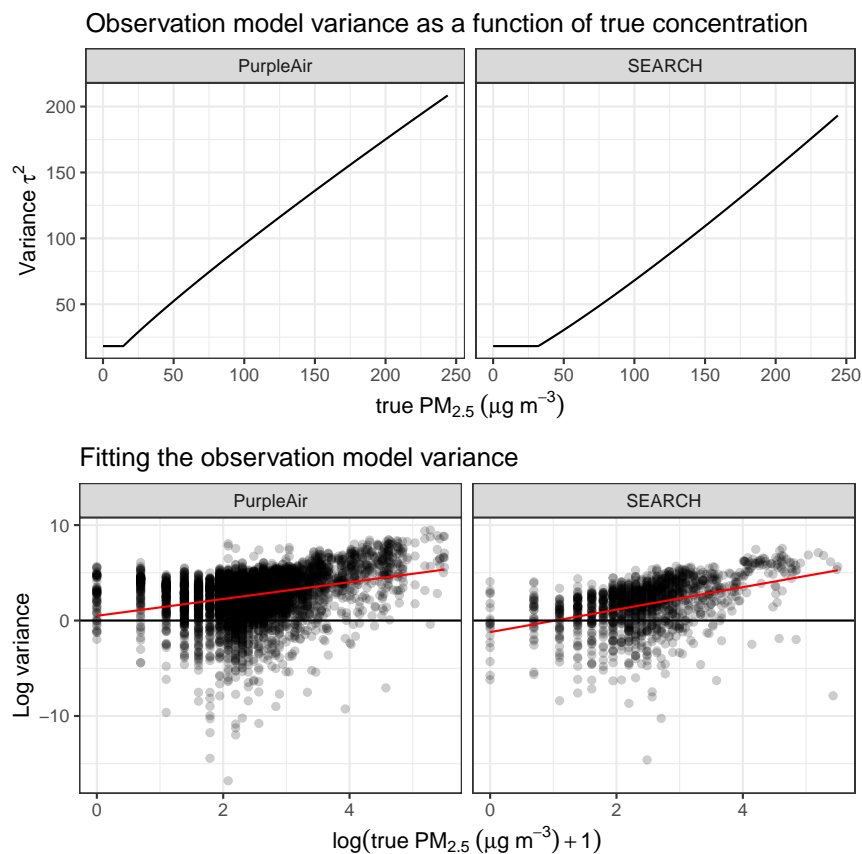


Figure S6: (Top) Variance of the observation model as a function of the true $\text{PM}_{2.5}$, for the two low-cost networks. (Bottom) Log variance of the observation model as a function of the log true $\text{PM}_{2.5}$, for the two low-cost networks, with points denoting the log squared bias of each observation during June and July 2023.

S3 Additional analysis of SEARCH and PurpleAir data

In Figure S7, we show the time series of true concentrations as measured at Lake Montebello.

Figure S8 presents one of the timepoints where the length of the confidence interval increases when two networks are used instead of one (see Figure 4). As we see in Figure S8 (top left), at many of these timepoints, the PurpleAir network predicts a very flat surface, with

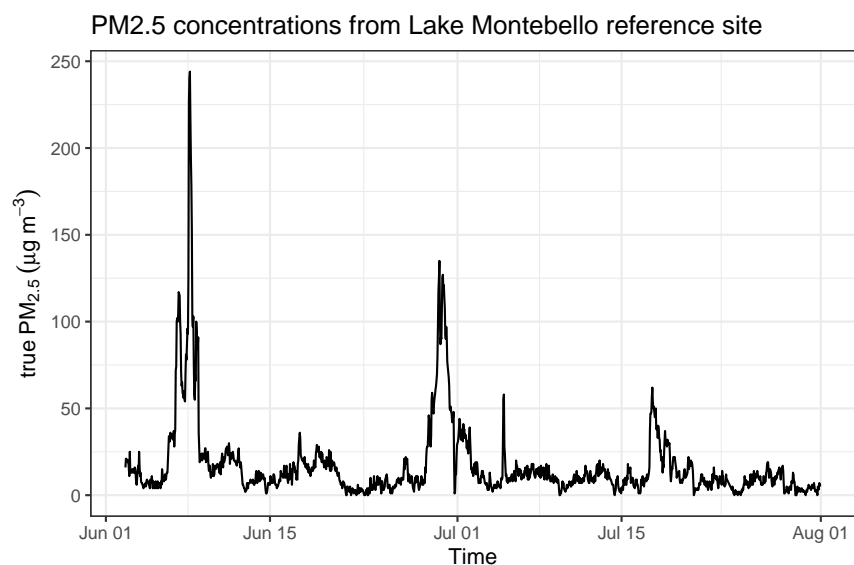


Figure S7: $PM_{2.5}$ at Lake Montebello in June and July 2023

low uncertainty (Figure S8 bottom left) at all locations in the city. The SEARCH network better captures variability, as seen from the wider confidence interval lengths in Figure S8 bottom middle. The variability of the maps produced from the two-network MGPF is also higher than the uncertainty from just using the PurpleAir network, as it incorporates the information from the SEARCH network.

We present some further diagnostics of the analysis of low-cost data in Baltimore. First, the absolute differences in CI lengths at the network sites and the interpolated locations are shown in Figures S9-S10. Also, the parameters of the Gaussian Process part of the MGPF are shown in Figure S11. The spatial variance and nugget terms are both larger when the GP mean is higher, which is during the peak periods. Outside of these periods, there are few timepoints where these variances are very large. Overall, the parameters look as expected, indicating that the selection of bounds and the model fit are adequate.

We also compare the predictions from the observation model and the spatial filtering methods

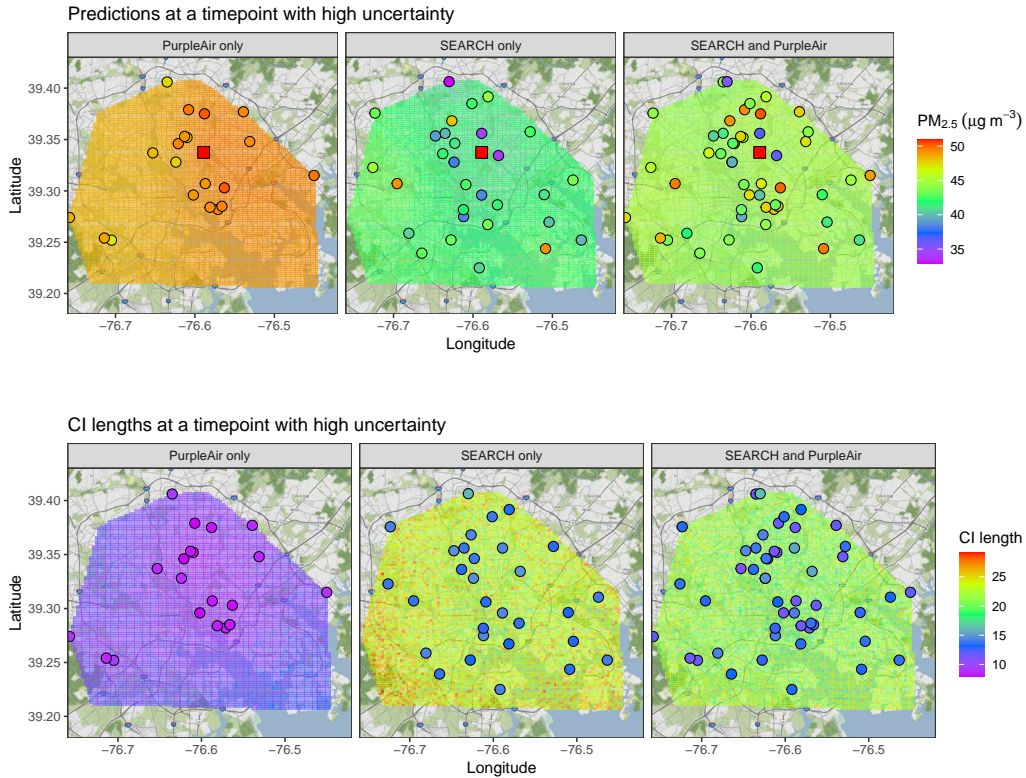


Figure S8: Map of the (top) predictions and (bottom) length of the confidence intervals, on June 30, 2023 at 10am. Circles represent low-cost network sites. The square represents the Lake Montebello site.

in Figure S12. We see that there is considerable fluctuation between the predictions, which means that there are many timepoints where the spatial model changes the naïve predictions from the observation model considerably, due to the added spatial information. Therefore, we do not see evidence of overly relying on the observation model for predictions. Also, the differences center around 0, indicating that the filtering does not systematically increase or decrease the prediction compared to the observation model.

In Figures S13-S14, we also present versions of Figures 5-6 that include the sensor sites as well as the interpolated sites. A few sensors have much higher or lower average than the majority of the network, so it is more difficult to see the city-wide pattern when including

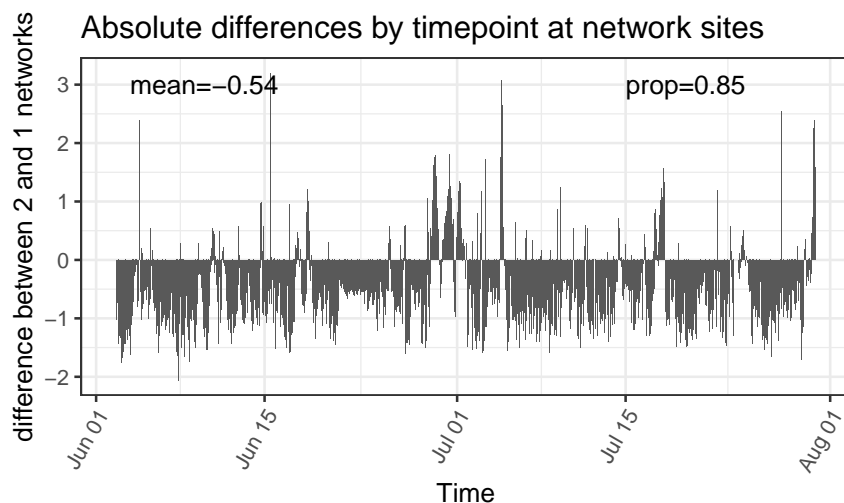


Figure S9: Absolute difference in CI lengths, for each timepoint, averaged across the PurpleAir and SEARCH networks. The median of the differences, and the proportion p of differences that are negative, are listed.

the sensor sites. Additionally, the CI lengths at the network sites are much smaller than at the interpolated sites because of the presence of the low-cost sensors and the inclusion of a nugget in the model.

We now focus on certain time periods: those with high/low $\text{PM}_{2.5}$ at Lake Montebello, and those where $\text{PM}_{2.5}$ is most/least variable across the city (Figure S15). Rather than looking at the raw variance, we consider the coefficient of variation, scaling the standard deviation of the predictions at network sites by the mean of the predictions, so that the high variance timepoints don't overlap too much with the high concentration timepoints. We look at the median percent difference in confidence interval lengths so that the results are not overly influenced by a few very large percent increases. For high concentration timepoints, adding the PurpleAir network to the SEARCH network decreases the CI length across the city by a median of 15%, while adding the SEARCH network to the PurpleAir network increases CI lengths, since the PurpleAir network tends to be overconfident at high concentrations,

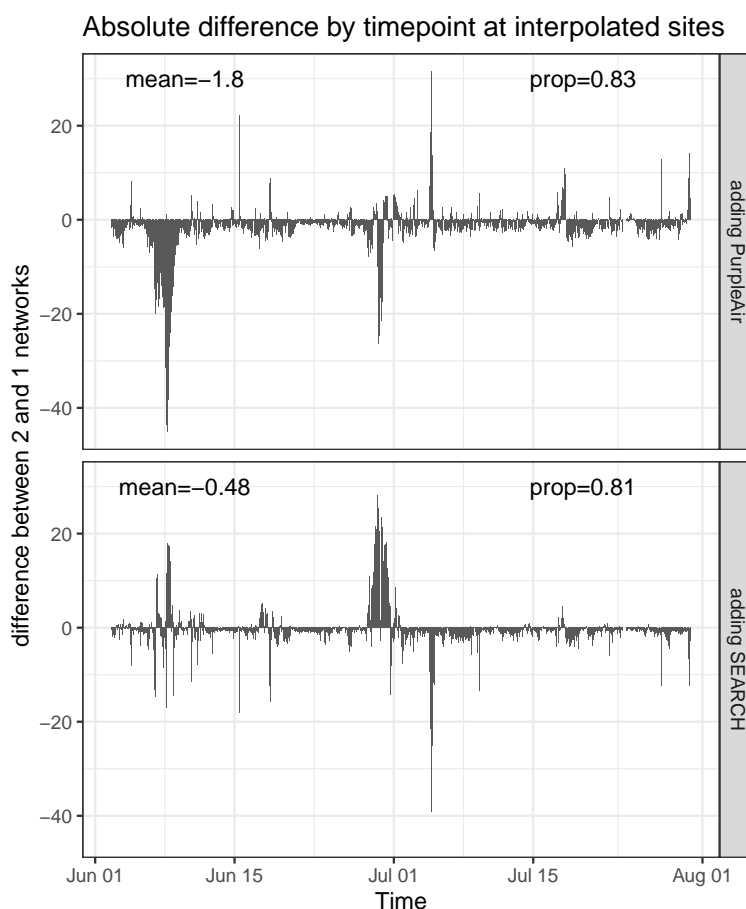


Figure S10: Difference in CI lengths averaged across all interpolated sites in Baltimore, using both networks compared to using only one network. The median of the differences, and the proportion p of differences that are negative, are listed.

since it tends to estimate flatter pollution surfaces. For low pollution timepoints, there is a decrease in uncertainty from adding both networks, but the greatest improvement is obtained from adding the SEARCH network, because PurpleAir alone tends to have wider intervals for these timepoints. For high or low variability timepoints, both networks contribute to a decrease in CI length, with adding the SEARCH network causing greater improvement for high variability timepoints, and adding PurpleAir a greater improvement for low variability timepoints, with up to a 30% reduction in uncertainty.

We present the maps of the average (Figure S16), and CI length (Figure S17) overall all timepoints. The previous maps separated out high and non-high timepoints. The same areas of the city, namely the east and southeast, have the highest concentrations and CI lengths averaging over all timepoints as when looking at high or non-high timepoints separately. We also present a map of the point estimates and uncertainty at one timepoint, June 7, 2023 at 7pm, in Figure S18. This timepoint was selected because it is one of the timepoints with high concentrations on average, but not the highest concentrations observed during this period. From these maps, we see that the issues of preferential sampling in the PurpleAir network and high uncertainty in the SEARCH network that were evident when averaging over the whole two month period are also present at individual timepoints.

We also show a comparison of the MGPF to individually calibrating each network and then interpolating using inverse distance weighting (IDW) (Mueller et al., 2004). Each network can be calibrated using a regression calibration model (RegCal) (Heffernan et al., 2023), which models the true concentration as a linear function of the low-cost measurement. Each network can have its own calibration equation, and then IDW can interpolate these values to all other locations in the city. The average predictions across the city using this method are shown in Figures S19 and S20), compared to the MGPF method. Since information is not shared across sites in the regression-calibration-followed-by-IDW method, there is much more local fluctuation across the city, and the locations of many of the sites are visible as local minimums or maximums in $PM_{2.5}$. It is unlikely that where the sensors were placed exactly corresponds to locations which has lowest or highest concentrations, and this is an artifact of the IDW interpolation.

Additionally, Heffernan et al. (2023) showed that these linear models tend to underestimate high concentrations, while the MGPF guards against this. Thus, at high concentrations,

the predicted concentrations from doing IDW on RegCal predictions are consistently and considerably lower than using the MGPF (Figure S21). This results in lower concentrations on average as well (Figure S19, Figure S20 (top)).

Finally, to quantitatively assess the accuracy of doing IDW on RegCal predictions on two networks compared to our MGPF method, we calculate a pseudo-RMSE. Since we only know the true $\text{PM}_{2.5}$ concentrations at Lake Montebello, we consider locations within a 3km radius of this site, and use the true concentrations measured at Lake Montebello as approximate proxy reference data at these nearby locations. The pseudo-RMSE across the two month period is shown in Figure S22. The figure shows both the RMSE at the network sites, and on the interpolated surface. We see that doing IDW on RegCal has much higher pseudo-RMSE than using the MGPF.

Parameter estimates over time

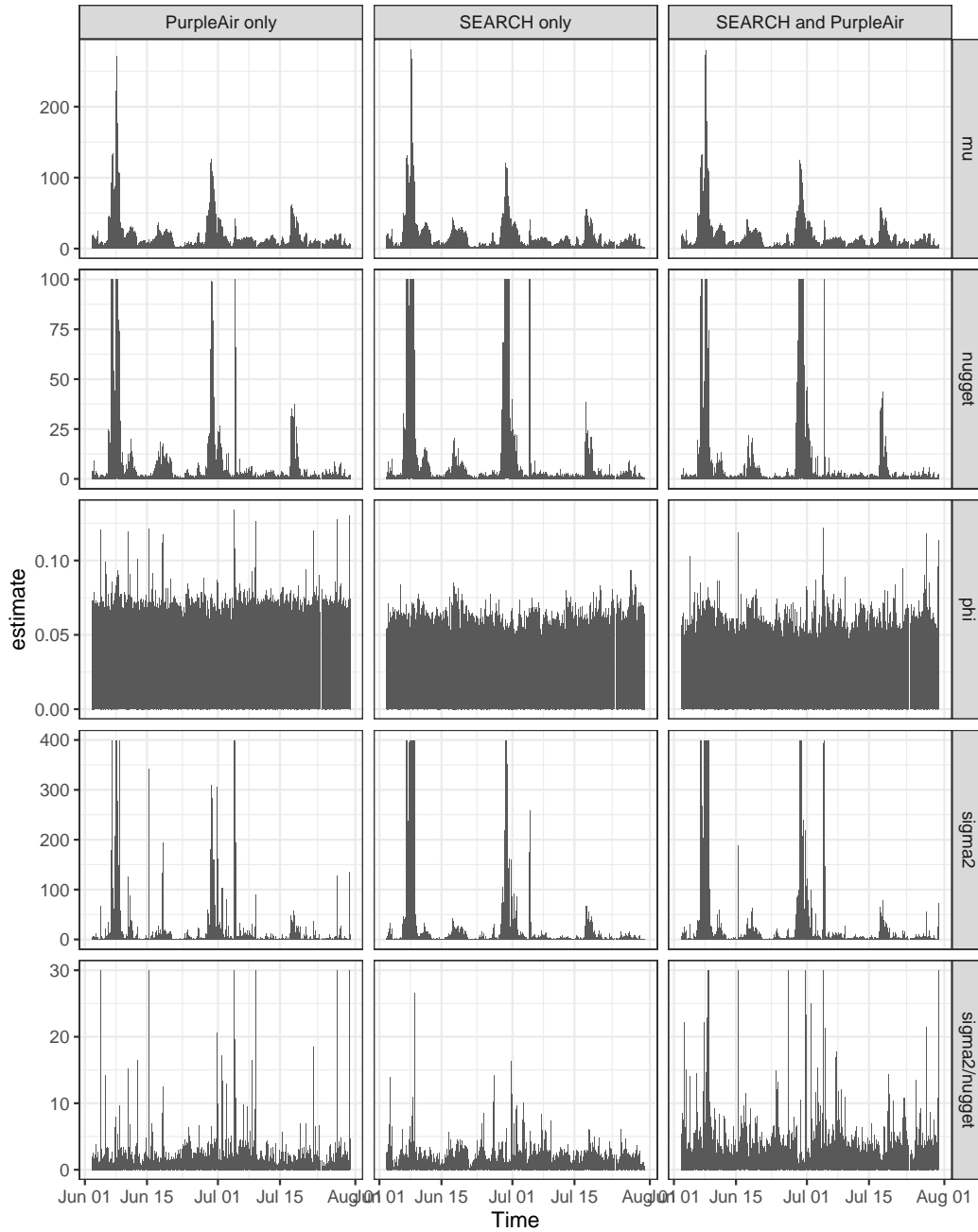


Figure S11: Hourly parameter estimates from the Gaussian Process model, when applying the MGPF to Baltimore data.

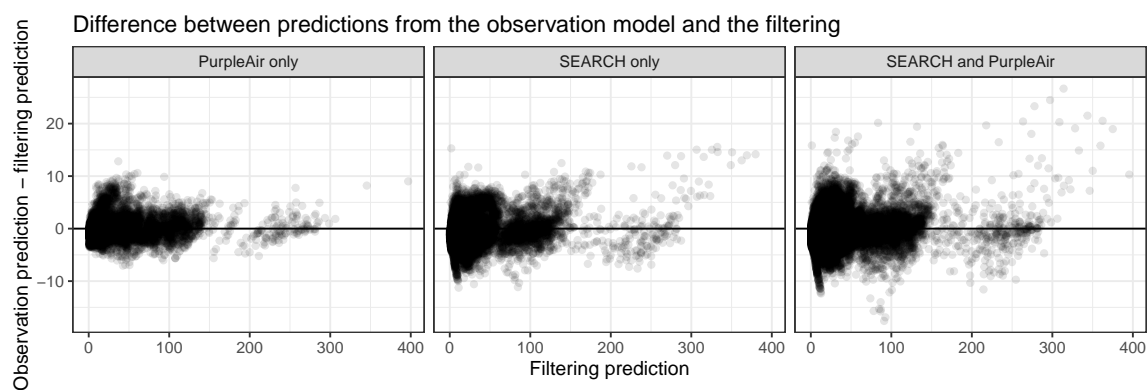


Figure S12: Comparison of the predictions from the observation model and from the GPF (left and center panels) and MGPF (right panel) spatial filtering.

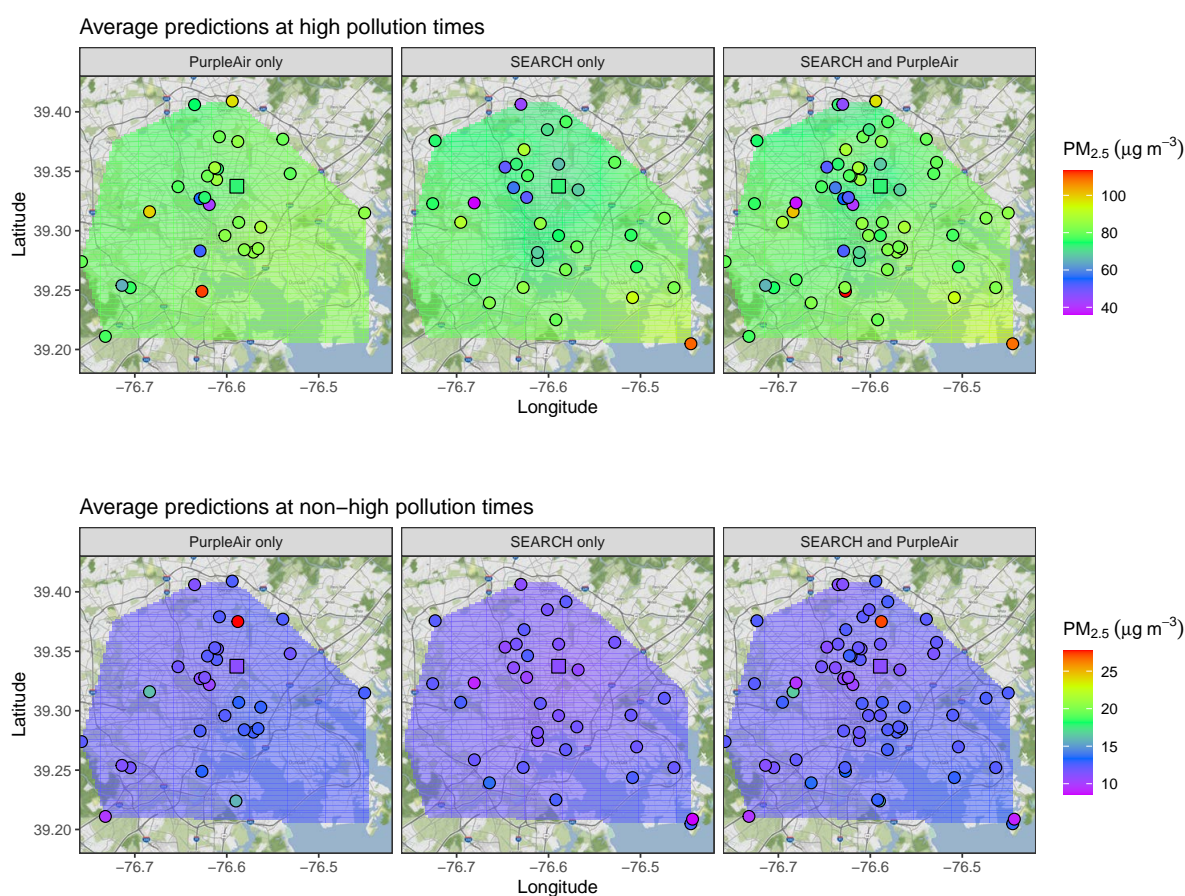


Figure S13: Mean of predicted $PM_{2.5}$ in Baltimore (Top) over the days with high pollution (Bottom) over all remaining days. Circles represent low-cost network sites. The square represents the Lake Montebello site.

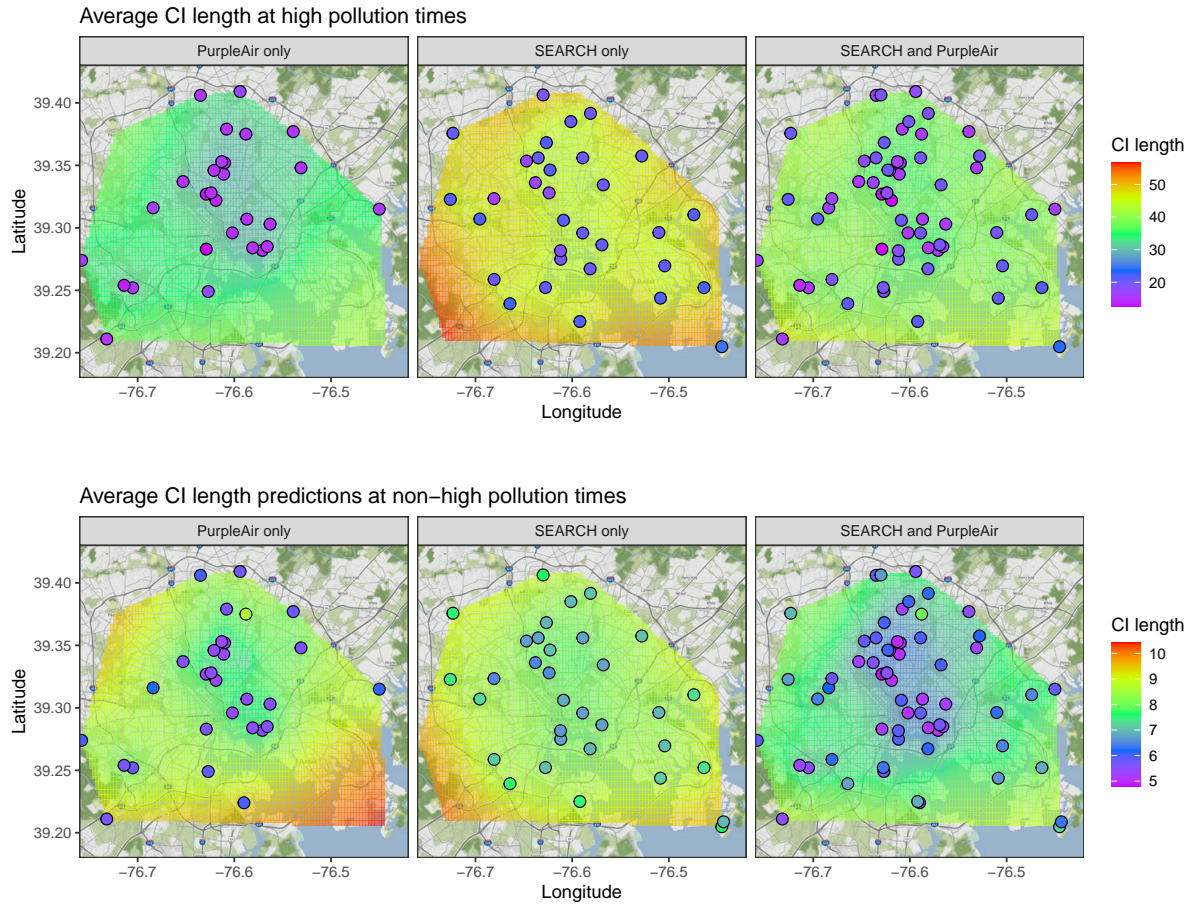


Figure S14: Average confidence interval length of predicted PM_{2.5} in Baltimore (Top) over the days with high pollution (Bottom) over all remaining days. Circles represent low-cost network sites.

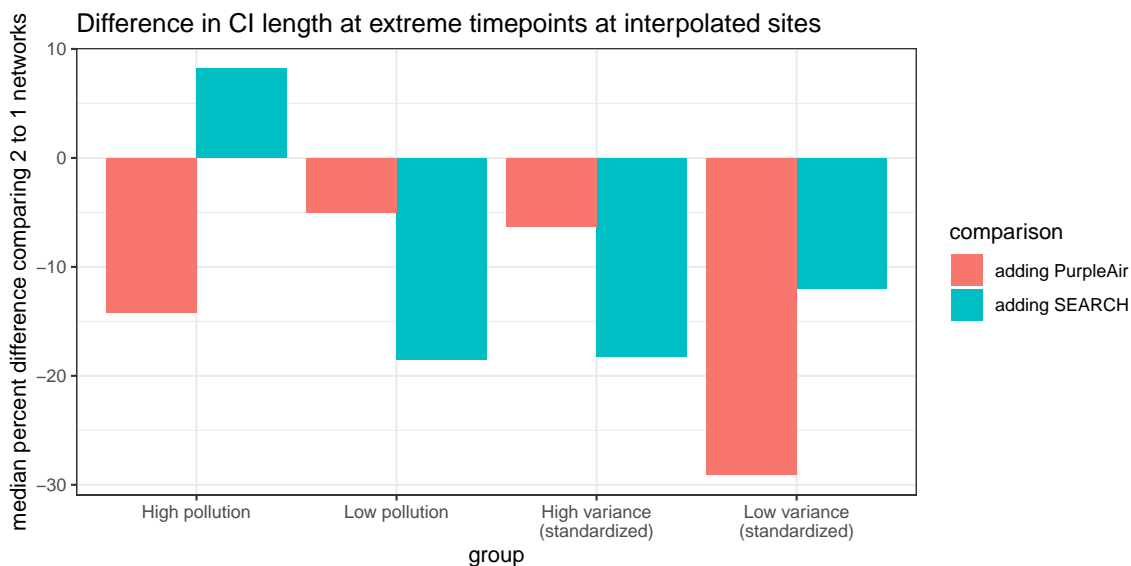


Figure S15: Median percent difference in CI lengths averaged across all interpolated sites in Baltimore, focusing on timepoints in the top/bottom 10% of concentrations at Lake Montebello or network-wide variability in predictions

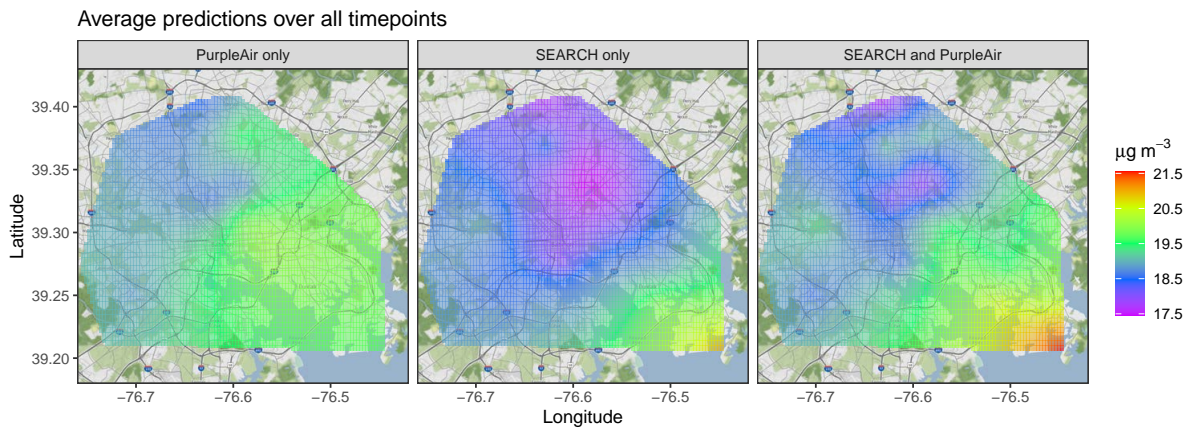


Figure S16: Mean of predicted $PM_{2.5}$ in Baltimore over all times in June and July 2023.

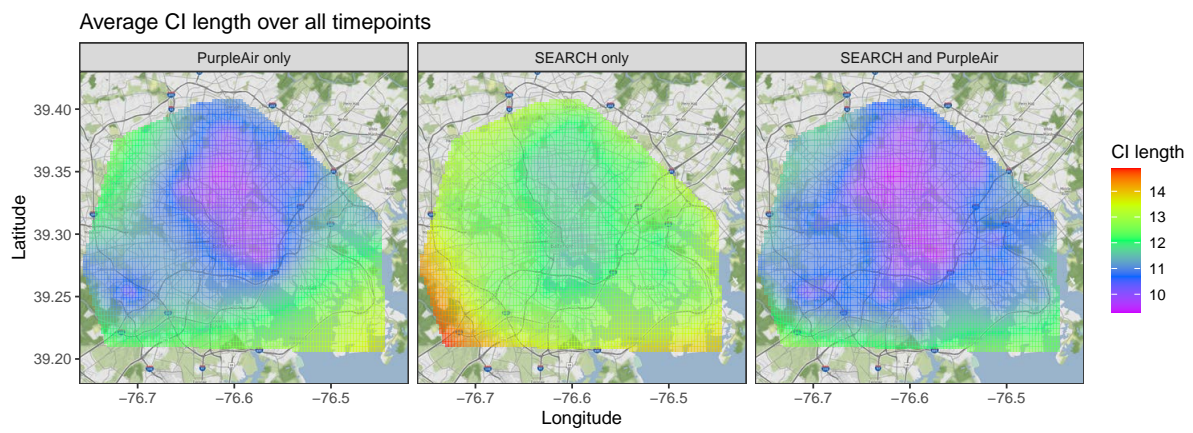


Figure S17: Average confidence interval length of predicted PM_{2.5} in Baltimore over all times in June and July 2023.

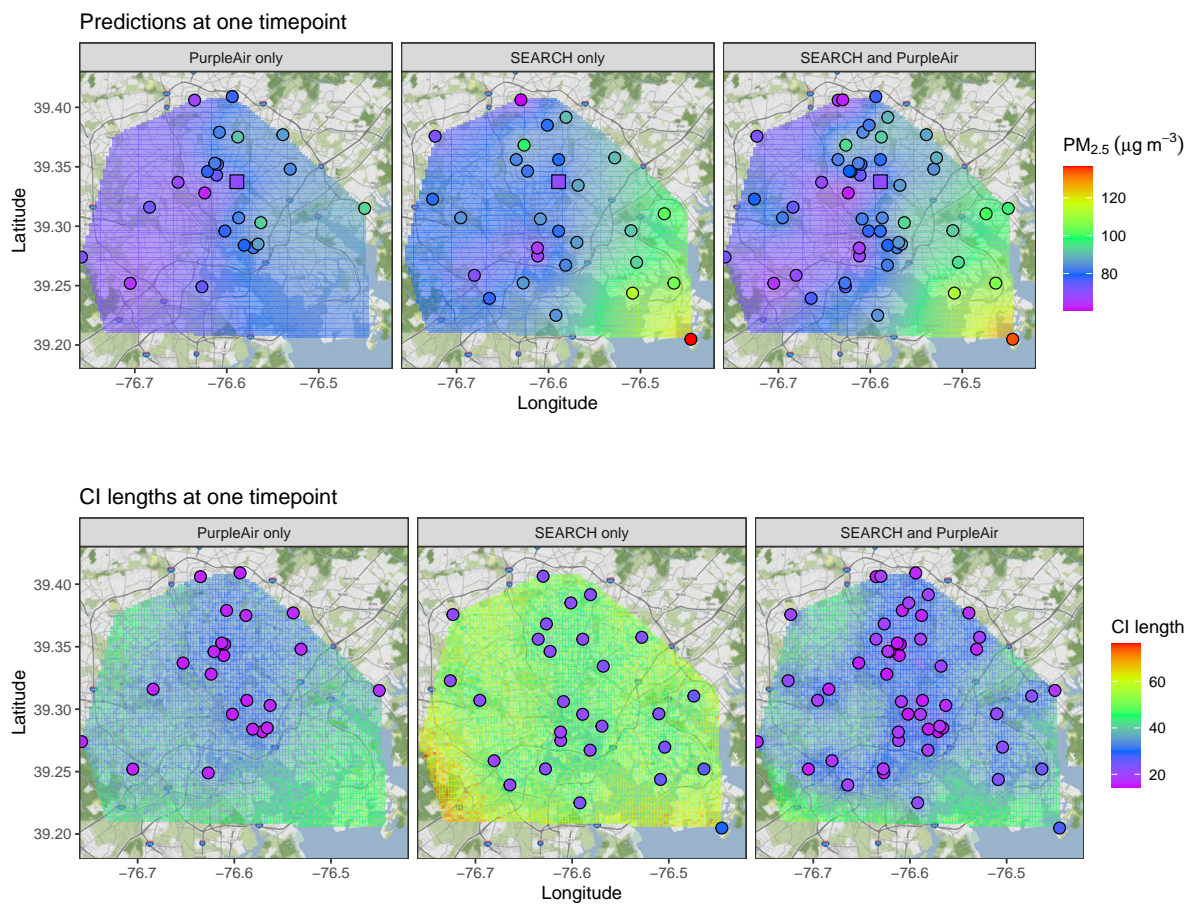


Figure S18: (Top) Predictions or (bottom) CI lengths, at one hour using one network or both. Circles represent low-cost network sites. The square represents the Lake Montebello site. The timepoint shown in these maps is June 7, 2023 at 7pm.

Average predictions over all timepoints

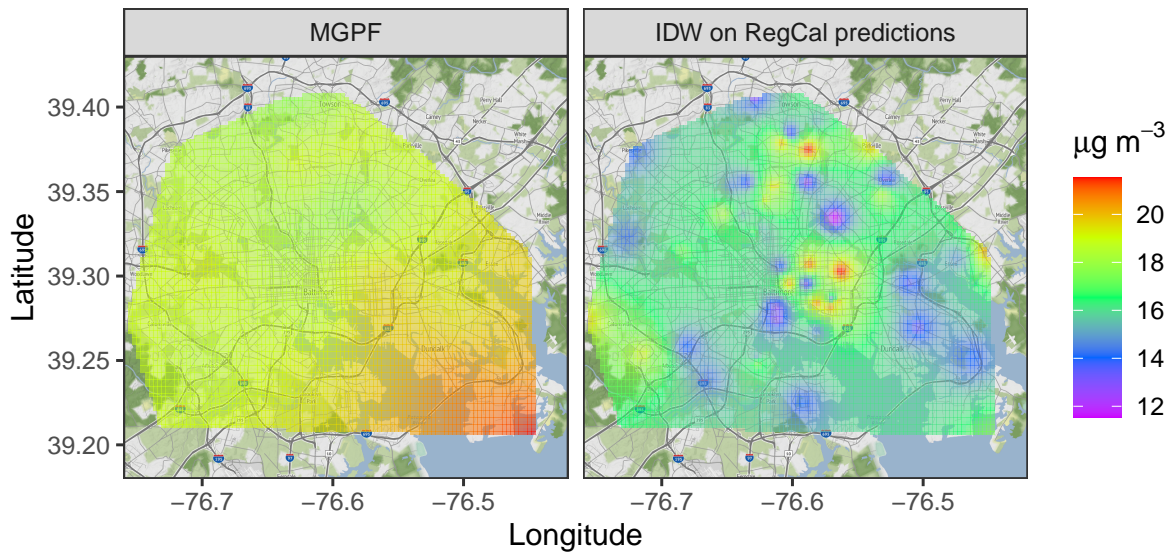


Figure S19: Average predicted PM_{2.5} in Baltimore over all times in June and July 2023, including using IDW on individual network calibrations

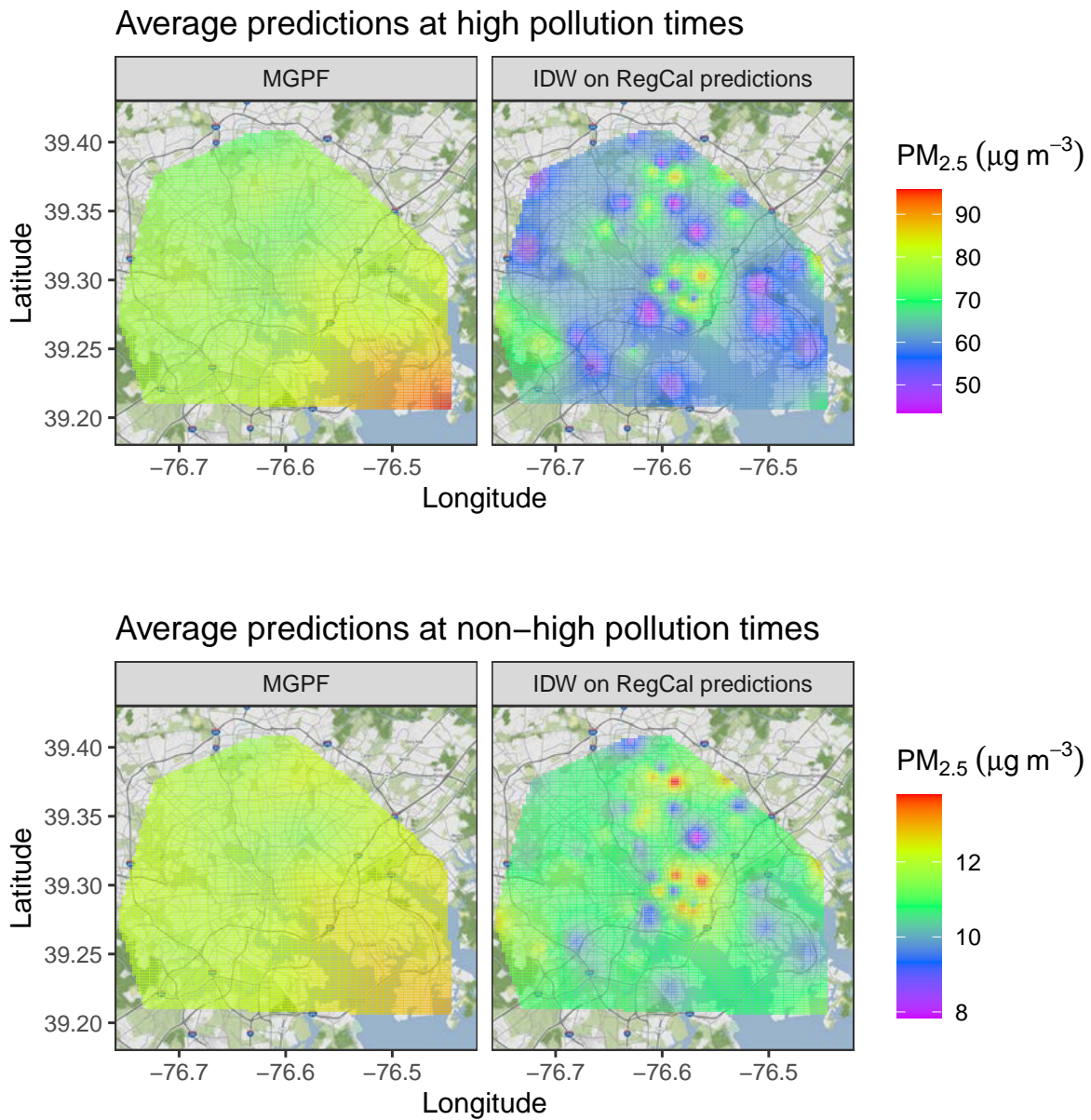


Figure S20: Average predicted PM_{2.5} in Baltimore (Top) over the days with high pollution (Bottom) over all remaining days in June and July 2023, including using IDW on individual network calibrations

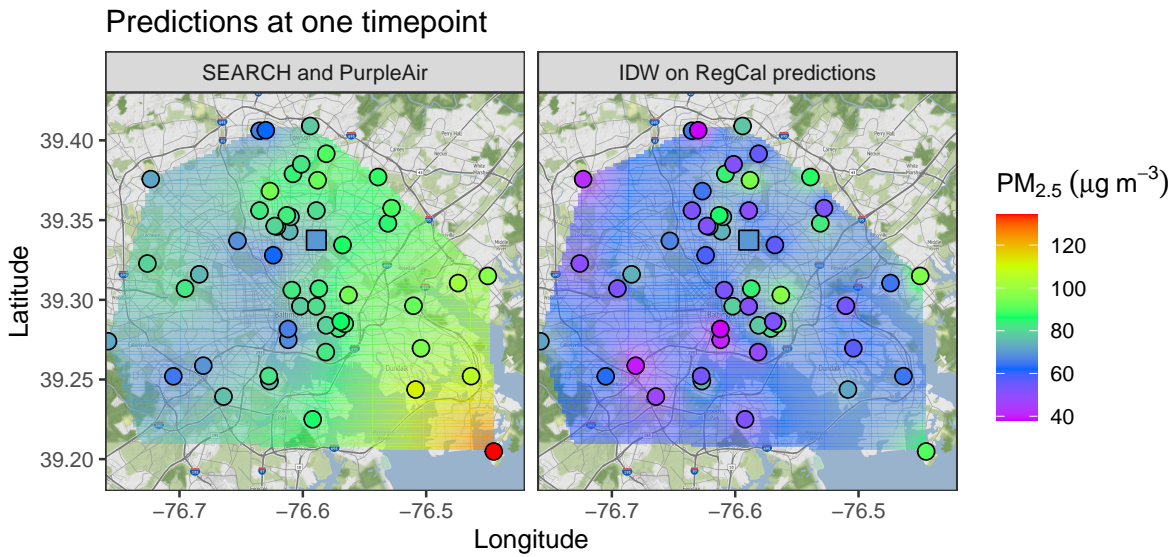


Figure S21: Average predicted PM_{2.5} in Baltimore during one timepoint, including using IDW on individual network calibrations

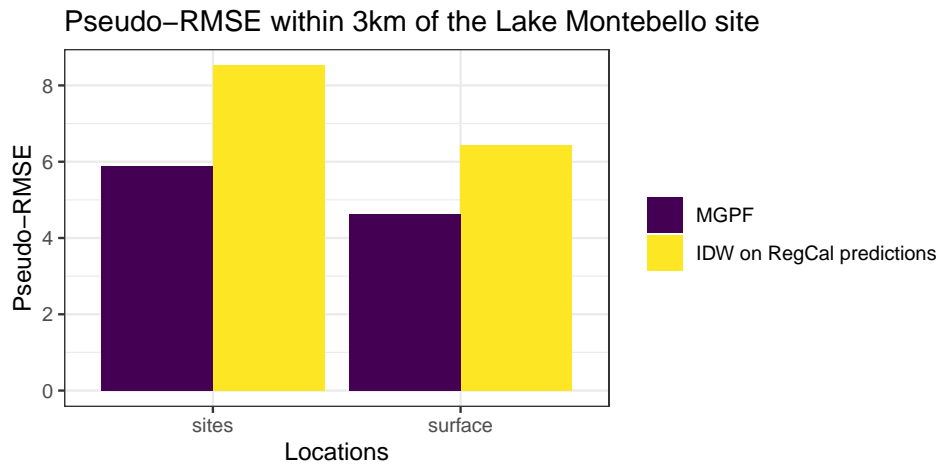


Figure S22: Pseudo-RMSE when using filtering on the SEARCH network, PurpleAir network, or both networks together, as well as using IDW on the predictions from regression calibration models (RegCal). Only sites or locations along the interpolated surface within 3km of Lake Montebello are considered.

S4 Details of simulation setup

For each dataset, we simulate locations from a unit square with point sources at $(0.2, 0.1)$ and $(0.9, 0.2)$. These point sources will be used to generate a local pollution surface. A single reference location is sampled from a smaller central square of length $1/3$. Then, for each network, 30 low-cost site locations are sampled. If there is no preferential sampling, these locations are all drawn from the full unit square. If there is preferential sampling, these locations are then transformed to be preferentially sampled as follows: the first 6 locations are left as is. The remaining 24 locations are restricted to being within the top-left quadrant of the unit square. Any location that was already in this quadrant is left unchanged, while for the remaining locations, the coordinate(s) that fall outside this quadrant are resampled. Then, a Gaussian Process is used to simulate a true ambient (background) concentration surface with means μ_t generated from a shifted Beta distribution with a minimum of 2 and most of the data below 12. The spatial scale parameter ϕ_t is generated so that the correlation at the farthest points across the network is high. The spatial variance σ_t^2 is also generated from a Beta distribution, scaled according to the value of μ_t , and the nugget variance $\sigma_{n,t}^2$ is restricted to being small relative to σ_t^2 . Once the ambient concentrations are generated from the GP, emissions from the point sources are generated. The emission at each source is generated from a shifted Beta distribution with minimum of 20, and most of the data under 180. The effect of the source decreases exponentially with respect to the squared distance from the source.

The sum of the ambient concentration (GP) and the local concentration (driven by the two

point source emissions) is the final concentration surface, which gives a final surface of:

$$\begin{aligned}
x(\mathbf{s}, t) &= x_{ambient}(\mathbf{s}, t) + x_{local}(\mathbf{s}, t) \\
x_{local}(\mathbf{s}, t) &= z_{1,t} \exp\{-d_{1,\mathbf{s}}^2 \psi_{1,t}\} + z_{2,t} \exp\{-d_{2,\mathbf{s}}^2 \psi_{2,t}\} \\
x_{ambient}(\cdot, t) &\sim GP(\mu_t, \sigma_t^2 \exp\{-\phi_t d\} + \sigma_{n,t}^2 \mathbb{I}_{d=0}) \\
z_{1,t} &\sim a_1 Beta(b_1, c_1) \\
z_{2,t} &\sim a_2 Beta(b_2, c_2)
\end{aligned}$$

where $d_{i,\mathbf{s}}$ is the distance from location \mathbf{s} to point source i .

We note that the true data generation process is thus misspecified with respect to MGPF. In the true DGP only part of the true concentration is a GP (the ambient part), whereas in MGPF the entire true concentration is modeled as a GP.

Relative humidity is then generated from a uniform distribution. One low-cost network uses the PurpleAir observation model coefficients, while the other one uses a multiple (1.5) of those coefficients. Then the low-cost sensor measurements are generated using a heteroscedastic observation model variance model with the standard deviation of network B equal to 1.5 times the standard deviation of network A. This gives the observation models:

$$\begin{aligned}
\mathbf{y}(\mathbf{S}_A, t) &= -10.97 + 1.91x(\mathbf{S}_A, t) + 0.16RH(\mathbf{S}_A, t) + \epsilon_A(\mathbf{S}_A, t), \\
\epsilon_A(\mathbf{S}_A, t) &= 10.0 + 0.5x(\mathbf{S}_A, t), \\
\mathbf{y}(\mathbf{S}_B, t) &= -16.46 + 2.86\mathbf{x}(\mathbf{S}_B, t) + 0.25\mathbf{z}(\mathbf{S}_B, t) + \epsilon_B(\mathbf{S}_B, t), \\
\epsilon_B(\mathbf{S}_B, t) &= 22.5 + 1.13x(\mathbf{S}_B, t).
\end{aligned}$$

References

- Anderson, C. M., Kissel, K. A., Field, C. B., and Mach, K. J. (2018). Climate change mitigation, air pollution, and environmental justice in california. *Environmental science & technology* **52**, 10829–10838.
- Ardon-Dryer, K., Dryer, Y., Williams, J. N., and Moghimi, N. (2020). Measurements of pm 2.5 with purpleair under atmospheric conditions. *Atmospheric Measurement Techniques* **13**, 5441–5458.
- Aubourg, M. A., Sawtell, G., Deanes, L., Fabricant, N., Thomas, M., Spicer, K., Wagar, C., Campbell, S., Ulman, A., and Heaney, C. D. (2023). Community-driven research and capacity building to address environmental justice concerns with industrial air pollution in curtis bay, south baltimore. *Frontiers in epidemiology* **3**,.
- Barkjohn, K. K., Gantt, B., and Clements, A. L. (2021). Development and application of a united states-wide correction for pm 2.5 data collected with the purpleair sensor. *Atmospheric Measurement Techniques* **14**, 4617–4637.
- Bi, J., Wildani, A., Chang, H. H., and Liu, Y. (2020). Incorporating low-cost sensor measurements into high-resolution pm2.5 modeling at a large spatial scale. *Environmental science & technology* **54**, 2152–2162.
- Bigi, A., Mueller, M., Grange, S. K., Ghermandi, G., and Hueglin, C. (2018). Performance of no, no 2 low cost sensors and three calibration approaches within a real world application. *Atmospheric Measurement Techniques* **11**, 3717–3735.

- Boone, C. G., Fragkias, M., Buckley, G. L., and Grove, J. M. (2014). A long view of polluting industry and environmental justice in baltimore. *Cities* **36**, 41–49.
- Datta, A., Saha, A., Zamora, M. L., Buehler, C., Hao, L., Xiong, F., Gentner, D. R., and Koehler, K. (2020). Statistical field calibration of a low-cost PM2.5 monitoring network in Baltimore. *Atmospheric Environment* **242**, 117761.
- DeSouza, P., Kahn, R., Stockman, T., Obermann, W., Crawford, B., Wang, A., Crooks, J., Li, J., and Kinney, P. (2022). Calibrating networks of low-cost air quality sensors. *Atmospheric Measurement Techniques* **15**, 6309–6328.
- Esie, P., Daepf, M. I., Roseway, A., and Counts, S. (2022). Neighborhood composition and air pollution in chicago: monitoring inequities with a dense, low-cost sensing network, 2021. *American Journal of Public Health* **112**, 1765–1773.
- Fuentes, M. and Raftery, A. E. (2005). Model evaluation and spatial interpolation by bayesian combination of observations with outputs from numerical models. *Biometrics* **61**, 36–45.
- Fuller, R., Landrigan, P. J., Balakrishnan, K., Bathan, G., Bose-O’Reilly, S., Brauer, M., Caravanos, J., Chiles, T., Cohen, A., Corra, L., et al. (2022). Pollution and health: a progress update. *The Lancet Planetary Health* **6**, e535–e547.
- Heffernan, C., Peng, R., Gentner, D. R., Koehler, K., and Datta, A. (2023). A dynamic spatial filtering approach to mitigate underestimation bias in field calibrated low-cost sensor air pollution data. *The Annals of Applied Statistics* **17**, 3056–3087.
- Jerrett, M., Burnett, R. T., Kanaroglou, P., Eyles, J., Finkelstein, N., Giovis, C., and Brook, J. R. (2001). A gis–environmental justice analysis of particulate air pollution in hamilton, canada. *Environment and Planning A* **33**, 955–973.

- Kim, J., Shusterman, A. A., Lieschke, K. J., Newman, C., and Cohen, R. C. (2018). The berkeley atmospheric co2 observation network: Field calibration and evaluation of low-cost air quality sensors. *Atmospheric Measurement Techniques* **11**, 1937–1946.
- Lee, A., Szpiro, A., Kim, S., and Sheppard, L. (2015). Impact of preferential sampling on exposure prediction and health effect inference in the context of air pollution epidemiology. *Environmetrics* **26**, 255–267.
- Levy Zamora, M., Xiong, F., Gentner, D., Kerkez, B., Kohrman-Glaser, J., and Koehler, K. (2018). Field and laboratory evaluations of the low-cost plantower particulate matter sensor. *Environmental science & technology* **53**, 838–849.
- Liang, Y., Sengupta, D., Campmier, M. J., Lunderberg, D. M., Apte, J. S., and Goldstein, A. H. (2021). Wildfire smoke impacts on indoor air quality assessed using crowdsourced data in california. *Proceedings of the National Academy of Sciences* **118**, e2106478118.
- MDE (2023). Ambient Air Monitoring Network Plan for Calendar Year 2023. Maryland Department of the Environment. https://mde.maryland.gov/programs/air/AirQualityMonitoring/Documents/MDNetworkPlanCY2023_draftforpublic.pdf.
- Miranda, M. L., Edwards, S. E., Keating, M. H., and Paul, C. J. (2011). Making the environmental justice grade: the relative burden of air pollution exposure in the united states. *International journal of environmental research and public health* **8**, 1755–1771.
- Mueller, T., Pusuluri, N., Mathias, K., Cornelius, P., Barnhisel, R., and Shearer, S. (2004). Map quality for ordinary kriging and inverse distance weighted interpolation. *Soil Science Society of America Journal* **68**, 2042–2047.

- Romero, Y., Velásquez, R. M. A., and Noel, J. (2020). Development of a multiple regression model to calibrate a low-cost sensor considering reference measurements and meteorological parameters. *Environmental Monitoring and Assessment* **192**, 1–11.
- Shaddick, G. and Zidek, J. V. (2014). A case study in preferential sampling: Long term monitoring of air pollution in the uk. *Spatial Statistics* **9**, 51–65.
- Si, M., Xiong, Y., Du, S., and Du, K. (2020). Evaluation and calibration of a low-cost particle sensor in ambient conditions using machine-learning methods. *Atmospheric Measurement Techniques* **13**, 1693–1707.
- U.S. Census Bureau (2024). Explore Census Data. U.S. Census Bureau. <https://data.census.gov/>.
- U.S. EPA (2024). Final Rule to Strengthen the National Air Quality Health Standard for Particulate Matter Fact Sheet. U.S. Environmental Protection Agency, Washington, DC. <https://www.epa.gov/system/files/documents/2024-02/pm-naaqs-overview.pdf>.
- WHO (2024). Air Pollution. World Health Organization. <https://www.who.int/health-topics/air-pollution>.
- Zimmerman, D. L. and Holland, D. M. (2005). Complementary co-kriging: spatial prediction using data combined from several environmental monitoring networks. *Environmetrics* **16**, 219–234.